**Final Report
Of
Algorithm Development with HIS Data
NASA Grant NAS5-31377
For the period of
January 1 1991 to December 14 2003**

By

AIRS Science Team Member Prof. William L. Smith & Associates

Report Summary

This AIRS Science Team member research grant project is to demonstrate the use of simulated and observed AIRS data, and also the airborne High-resolution Interferometer Sounder (HIS) measurements as surrogate data for the improved mesoscale weather analysis and forecasting through the amalgamated use of high spectral (vertical) resolution infrared sounding data, and multispectral high spatial resolution quantitative imagery.

Prelaunch data requirements include NASA ER2 HIS and MAS measurements together with simultaneous ground truth (radiosonde) observations. After AIRS measurement and retrieval algorithm development and validation, the operational utility of AIRS sounding products for various weather forecasting applications are also the additional study to be achieved.

Major accomplishments during the period of this research are summarized below:
1) The continuous support of AIRS science team activities including conducting major filed experiments to collect valuable surrogate and in-situ data to demonstrate and develop processing algorithms that are suitable for AIRS and its imaging counterpart.
2) The development of independent processing approach to unambiguously and synergistically demonstrate the high spatial resolution processing of cloud contaminated sounding data.
3) Publications of algorithms and processing approaches developed under this grant for the operational processing of regional AIRS/MODIS data.
4) Validation of AIRS measurements and products through the analysis of field experimental data sets.

Background and Detail of the Report

This AIRS Science Team research grant is to contribute to the AIRS execution phase in several ways:

1) To provide radiance spectra observed from aircraft with coincident surface and radiosonde ground truth data, which can be used to test and refine AIRS data processing algorithms prior to and after the launch of the EOS Aqua platform.

2) To refine the computational efficient linear retrieval algorithm and implement a complete system for the routine processing of amalgamated AIRS/AMSU/MODIS sounding data.

3) To conduct joint studies to assess the operational utility of the AIRS data.

4) And most importantly, to support AIRS Science Team activities including conducting field experiments, science team meetings, and evaluation and validation of AIRS performance.

A complete bibliography of peer-reviewed publications in support of the AIRS program is included at the end of this report. As examples, the publications dealing with the use of actual AIRS data since the launch of the Aqua satellite in May 2002 are included in an Appendix to this report and summarized below. However, the complete list of PI publications related to the physics required for AIRS data processing, as provided at the end of this report, more adequately describe the breadth of the contributions and achievements been made under this project.

Example Accomplishment-1 (Appendix 1): An alternative to the AIRS science team algorithm has been developed and demonstrated and validated through its application to polar orbiting satellite AIRS spectrometer and high altitude aircraft NAST interferometer sounding radiance spectra. The algorithm is extremely real-time computationally efficient and is therefore applicable the very high data rate Geostationary Imaging Fourier Transform Spectrometer to follow AIRS. GIFTS hyperspectral instrument will provide high spatial and temporal resolution temperature and moisture soundings from geosynchronous orbit from which wind profiles can be determined. Full exploitation of the GIFTS will rely on the assimilation of its continuous data stream in numerical weather prediction models.

The research performed under AIRS Science Team grant has fostered the advancement of processing system alternatives for the AIRS as well as generation geosynchronous sounding applications.

Example Accomplishment-2 (Appendix 2): Cloud greatly complicates the interpretation of infrared sounding data. The new hyperspectral resolution infrared sounding systems alleviate much of the ambiguity between cloud and atmospheric temperature and moisture contributions. However, in heavily clouded situations, the thermodynamic profile information to be retrieved is limited to the atmosphere above clouds. The results of the study presented here indicate some success in the ability to retrieve information below scattered and partially transparent Cirrus cloud (i.e., clouds with effective optical depths of less than unity). The thermodynamic profile information can be obtained by a combination of cloud clearing and by direct retrieval from the clouded radiances using a

realistic cloud radiative transfer model. Results achieved with airborne NAST-I and Aqua satellite AIRS observations show that accuracies close to those achieved in totally cloud-free conditions can be achieved down to cloud top levels. The accuracy of the profile retrieved below cloud top level is dependent upon the optical depth and fractional coverage of the cloud.

For the assimilation of cloudy radiances into an NWP model, two approaches might be considered: (1) an indirect method whereby clear sky equivalent radiances are assimilated, and (2) a direct method in which the actual cloud radiances are assimilated. For the indirect method, a combined EOF regression retrieval followed by a 1-d variational retrieval, using the cloud parameters from the EOF regression retrieval, is performed and the results above the highest cloud level with an effective optical depth greater than one is amalgamated with the model profile to recompute the equivalent clear sky radiances for the hybrid atmospheric profile condition. One can then assimilate the "clear" radiance whose weighting functions peak above the derived cloud level.

Thus, this research study, partially supported by AIRS Science Team grant, addresses the fundamental needs for treatment of clouds that greatly contaminate the infrared measurements that are measured by the AIRS. The optimal use of AIRS cloudy data will be significantly improved as a result of this study effort. The cloudy scene sounding and cloud parameter retrieval algorithm developed here is planned to be applied to global AIRS data obtained from the Aqua satellite in support of the NCEP assimilation of AIRS cloudy radiance measurements.

Example Accomplishment-3 (Appendix 3): This publication documents the findings, characteristics, and assessment of cloud affected AIRS measurements in measurements, cloud-cleared radiances and their respected applications. The results are helping to accelerate the understanding of the cloud signature and its implications of direct sounding and indirect assimilation in the NWP models.

Example Accomplishment-4 (Appendix 4): The applicability of this hyperspectral cloud property retrieval technique is demonstrated using the aircraft–based HIS data from the SUCCESS in 1996 and FIRE-ACE in 1998. Accurate cloud property retrievals for relatively large (45 μm) and small (12.5 μm) effective particle sizes can be achieved using a simultaneous retrieval approach which provides a fit of radiance calculations to the observed radiance spectra. Spectral temperature differences of ~4 degree and >20 degree Kevin (the slope of the spectral brightness temperatures and wavenumber between 790–960 cm^{-1}) further demonstrate that the forward modeling of cloudy measurements and the cloudy sky retrieval algorithm are capable of obtaining reliable cloud property estimates as needed for the cloudy radiance assimilation process. Subsequent cloud modeling study and retrieval analysis verification using space-borne and active cloud measurements, and *in-situ* measurements are being conducted to advance this technique as a prelude to its implementation in the operational numerical analysis/forecast system. The algorithm is now been used to process AIRS cloudy data and to retrieve global microphysical property of ice clouds. As a result of this and other studies performed

under the AIRS Science Team grant, our knowledge of the impact of clear and cloudy sky on the global radiation budget and cloud thermal dynamics for which NWP model requires reliable initial clouds and sounding information, has been greatly increased.

Summary

The research performed under the University of Wisconsin AIRS Science Team grant has greatly increased are understanding of the physical processes effecting the interpretation of Aqua AIRS, as well as other, hyperspectral sounding radiance measurements. A large number of peer-reviewed publications have resulted from this research that are serving to convey this knowledge to scientists responsible for the processing of AIRS, and subsequent satellite, hyperspectral resolution sounding measurements. Advances in the numerical prediction of global weather are now being achieved through the assimilation of AIRS radiance data. Such advances can be attributed, in part, to the knowledge gained as a result of AIRS science team investigations, such as those performed under this grant.

PI Publications In Support of AIRS Project

Huang, H.-L., W. L. Smith, and H. M. Woolf, 1992: Vertical resolution and accuracy of atmospheric infrared sounding spectrometers. J. Appl. Meteor. 31, 265-274.

Smith, W. L., 1992: Future Space-Based Sounding Observations for Weather Analysis and Forecasting. Advances in Space Research (ISSN 0273-1177), Vol. 12, No. 7, 175-178.

Ackerman, S. A., E. W. Eloranta, C. J. Grund, R. O. Knuteson, H. E. Revercomb, W. L. Smith, and D. P. Wylie, 1993: University of Wisconsin cirrus remote sensing pilot experiment. BAMS, 74, 1041-1049.

Ackerman, S. A., W. L. Smith, and H. E. Revercomb, 1993: Comparison of Broadband and High-spectral resolution infrared observations. Int. J. Remote Sensing, Vol. 287-2882.

Murty, D. G. K., W. L. Smith, H. M. Woolf, and C. M. Hayden, 1993: Comparison of radiances observed from satellite and aircraft with calculations by using two atmospheric transmittance models. Applied Optics, 32(9), 1620-1628.

Smith, W. L., X. L. Ma, S. A. Ackerman, H. E. Revercomb, and R. O. Knuteson, 1993: Remote Sensing Cloud Properties from High Spectral Resolution Infrared Observations. J. Atmos. Sci., Vol. 50, 1708-1720.

McMillan, W.W.; Strow, L.L.; Smith, W.L.; Revercomb, H.E.; Huang, H.L.; Thompson, A.M.; McNamara, D.P., and Ryan, W.F. Remote sensing of carbon monoxide over the continental United States on September 12-13 1993. *Journal of Geophysical Research* 102(D9), 1997, pp10695-10709.

Diak, G. R., C. J. Scheuer, M. S. Whipple, and W. L. Smith, 1994: Remote Sensing of Land-Surface Energy Balance Using Data from the High-resolution Interferometer Sounder (HIS): A Simulation Study. Rem. Sens. Env., April, 106-118.

LeMarshall, J. F., P. A. Riley, B. J. Rouse, G. A. Mills, Z.-J. Wu, P. K. Stewart, and W. L. Smith, 1994: Real-time Assimilation and Synoptic Application of Local TOVS Raw Radiance Observations. Aust. Met. Mag., September, 153-166.

Theriault, J.-M. P. L. Roney, D. St.-Germain, H. E. Revercomb, R. O. Knuteson, and W. L. Smith, 1994: Analysis of the FASCODE Model and its H_2O Continuum Based on Long-Path Atmospheric Transmission Measurements in the 4.5-11.5 μ m Region. Applied Optics, January, 323-333.

Ackerman, S. A., W. L. Smith, A. D. Collard, X. L. Ma, H. E. Revercomb and R. O. Knuteson, 1995: Cirrus Cloud Properties Derived from High-spectral Resolution Infrared Spectrometry during FIRE II. Part II - Aircraft HIS Results. J. Atmos. Sci., 52(23), 4246-4263.

Collard, A. D., S. A. Ackerman, W. L. Smith, X. Ma, H. E. Revercomb, R. O. Knuteson and S.-C. Lee, 1995: Cirrus Cloud Properties Derived from High-spectral Resolution Infrared Spectrometry during FIRE II. Part III - Ground-based HIS Results. J. Atmos. Sci., 52(23), 4264-4275.

McKeown, W., F. Bretherton, H. L. Huang, W. L. Smith, and H. E. Revercomb, 1995: Sounding the Skin of Water: Sensing Air-Water Interface Temperature Gradients with Interferometry. Journal of Atmospheric and Oceanic Technology, 12, 1313-1327.

Smith, W. L., H. E. Revercomb, R. O. Knuteson, F. A. Best, R. Dedecker, H. B. Howell, and H. M. Woolf, 1995: Cirrus Cloud Properties Derived from High-spectral Resolution Infrared Spectrometry during FIRE II. Part I - The High resolution Interferometer Sounder (HIS) Systems. J. Atmos. Sci., 52(23), 4238-4245.

McMillan, W. W., L. L. Strow, W. L. Smith, H. E. Revercomb, and H. L. Huang, 1996: The Detection of Enhanced Carbon Monoxide Abundances in Remotely Sensed Infrared Spectra of a Forest Fire Smoke Plume. Geophysical Research Letters, 23(22), 3199-3202.

Smith, W. L., R. O. Knuteson, H. E. Revercomb, W. Feltz, H. B. Howell, W. P. Menzel, N. Nalli, O. Brown, P. Minnett, J. Brown, and W. McKeown, 1996: Observations of the Infrared Radiative Properties of the Ocean - Implications for the Measurement of the Sea Surface Temperature via Satellite Remote Sensing. Bull. Amer. Meteor. Soc., 77(1) Jan., 41-51.

Smith, W. L., H.-L. Huang, and Joe A. Jenney, 1996: An Advanced Sounder Cloud Contamination Study. J. Appl. Met., 35 (8), August 1996, 1249-1255.

Wu, X. and W. L. Smith, 1996: Sensitivity of Sea Surface Temperature Retrieval to Sea Surface emissivity. ACTA Meteor. Sinica, 10 (3), 376-384.

McMillan, W. W., L. L. Strow, W. L. Smith, H. E. Revercomb, H. L. Huang, A. M. Thompson, D. P. McNamara, W. F. Ryan, 1997: Remote sensing of carbon monoxide over the continental United States on September 12-13, 1993. Journal of Geophysical Research, **102**, 10695-10709.

Wu, X. and W. L. Smith, 1997: Emissivity of rough sea surface for 8-13 μm: modeling and verification. Applied Optics, 36 (12), 2609-2619.

Nalli, N. R., W. L. Smith, 1998: Improved Remote Sensing of Sea Surface Skin Temperature Using a Physical Retrieval Method. Journal of Geophysical Research, 103, C5, 10,527-10,542.

Smith, W. L, S. Ackerman, H. E. Revercomb, H. Huang, D. H. DeSlover, W. F. Feltz, L. Gumley, and A. Collard, 1998: Infrared Spectral Absorption of Nearly Invisible Cirrus Clouds. Geophysical Research Letters, 25, 1138-1140.

Strow, L.L.; Tobin, D.C.; McMillan, W.W.; Hannon, S.E.; Smith, W.L.; Revercomb, H.E. and Knuteson, R.O. Impact of a new water vapor continuum and line shape model on observed high resolution infrared radiances. *Journal of Quantitative Spectroscopy and Radiative Transfer* 59(3-5), March-May 1998, pp303-317.

Smith, W. L. , W. F. Feltz, R. O. Knuteson, H. R. Revercomb, H. B. Howell, Harold H. Woolf, 1999: The Retrieval of Planetary Boundary Layer Structure Using Ground Based Infrared Spectral Radiance Measurements. *Journal of Atmospheric and Oceanic Technology*, 16, 323-333, March 1999.

Ma, X. L., W. L. Smith, and T. J. Schmit, 1998: A Non-Linear Physical Retrieval Algorithm - Its Application to the GOES-8/9 Sounder. Journal of Applied Meteorology: Vol. 38, No. 5, pp. 501–513.

DeSlover, D. H., W. L. Smith, P. Piironen, and E . Eloranta, 1999: A Methodology for Measuring Cirrus Cloud Visible to Infrared Spectral Optical Depth Ratios. Journal of Atmospheric and Oceanic Technology, 16(2), February 1999, pp251-262.

D. K. Zhou, W. L. Smith, and A. M. Larar, "Surface temperature and emissivity from airborne measurements of IR radiance spectra," *Eos Trans. AGU*, **82**(47) (2001).

Nalli, Nicholas R., Smith, William L., and Huang, Bormin, 2001. Quasi-specular model for calculating the reflection of atmospheric-emitted infrared radiation from a rough water surface. Applied Optics 40 (9), March 2001, pp1343-1353.

Huang, Bormin, William L. Smith, Hung-Lung Huang, and Harold M. Woolf, 2002: Comparison of linear forms of the radiative transfer equation with analytical jacobians. *Applied Optics* Vol 42, No 21 pp4209-4219.

Zhou D. K., W. L. Smith, and A. M. Larar. 2002. Thermodynamic product retrieval methodology for NAST-I and validation. *Applied Optics* Accepted for publication. In press.

Zhou, D. K., and W. L. Smith, "Surface emissivity effects on geophysical retrieval of IR spectral radiance", to be submitted to the *Geophys. Res. Lett.*, 2003

Smith, W. L., D.K. Zhou, H. E. Revercomb, H. L. Huang, P. Antonelli, and S. A. Mango, 2003: "Hyperspectral Atmospheric Sounding", Proceedings of the SPIE 10th International Symposium on Remote Sensing, Barcelona Spain, 8-12 September, 2003

Smith, W. L., and D. K. Zhou, H-L Huang, Jun Li, X. Liu, and A. M. Larar, 2004: "Extraction of Profile Information from Cloud Contaminated Radiances", Proceedings of the ECMWF Workshop on the Assimilation of High Spectral Resolution Sounders in NWP, June 28 July 1, 2004.

Huang, H-L, P. Yang, H.-L. Wei, B. A. Baum, Y.-X. Hu, P. Antonelli, and S. A. Ackerman, "Retrieval of ice cloud properties from high spectral resolution infrared observations," *IEEE Trans. Geosci. Remote Sensing*, vol. 42, pp. 842-853, 2004.

H. L. Huang, and W. L. Smith, "Apperception of clouds in AIRS data", ECMWF *Workshop on Assimilation of high spectral resolution sounders in NWP,* 28 June – 1 July 2004, ECMWF, Shinfield Park, p.155 – 169, 2004.

Hyper-spectral Atmospheric Sounding

W. L. Smith[a], D. K. Zhou[a], H. E. Revercomb[b], H. L. Huang[b], P. Antonelli[b], and
S. A. Mango[c]

[a]AtSC, NASA Langley Research Center, Hampton, VA 23681; [b]SSEC,
University of Wisconsin–Madison, Madison, WI 53706; [c]NPOESS Integrated
Program Office,
Silver Spring, MD 20910

ABSTRACT

Abstract. The Geosynchronous Imaging Fourier Transform Spectrometer (GIFTS) is the
first hyper-spectral remote sounding system to be orbited aboard a geosynchronous
satellite. The GIFTS is designed to obtain revolutionary observations of the four
dimensional atmospheric temperature, moisture, and wind structure as well as the
distribution of the atmospheric trace gases, CO and O_3. Although GIFTS will not be
orbited until 2006-2008, a glimpse at the its measurement capabilities has been obtained
by analyzing data from the National Polar-orbiting Operational Environmental Satellite
System (NPOESS) Airborne Sounder Test-bed- Interferometer (NAST-I) and Aqua
satellite Atmospheric Infrared Sounder (AIRS). In this paper we review the GIFTS
experiment and empirically assess measurement expectations based on meteorological
profiles retrieved from the NAST aircraft and Aqua satellite AIRS spectral radiances.

1. INTRODUCTION

Background: The Geosynchronous Imaging Fourier Transform Spectrometer (GIFTS)
was selected for NASA's New Millennium Program (NMP) Earth Observing-3 (EO-3)
mission. The GIFTS combines new and emerging sensor and data processing
technologies to make geophysical measurements that will contribute to earth science, as
well as lead to revolutionary improvements in meteorological observations and
forecasting. This mission will validate the GIFTS measurement concept for altitude-
resolved "water vapor winds" and demonstrate revolutionary technologies for future
research and operational systems. The infusion of GIFTS technologies into operational
instrumentation is critical for optimizing the next generation geostationary weather and
climate observing system.

The GIFTS program is made possible by a NASA, NOAA, and Department of
Defense partnership to share costs for instrument development, launch services,
validation of sensor capability, and ground data reception and processing of the sounding
data. The current plan is to complete the GIFTS instrument in late 2005 to support a
2006 to 2008 launch opportunity. The GIFTS satellite and its associated launch date

remain to be finalized. The first 12 months of operation will be conducted by NASA to satisfy the technology and measurement concept validation phase of the NMP EO-3 mission. During this time period, NOAA will also conduct, in near real-time, a demonstration of operational forecast utility of the GIFTS data. This first year period of operation is important for supporting the infusion of GIFTS technology and data processing techniques into the future operational GOES-R system. After the validation and demonstration phase, the GIFTS operation will be transferred to a geographical position dictated by the satellite provider for another 5-7 years of routine operation. The intent is to use the GIFTS data for Earth Observing System (EOS) scientific research and operational weather forecasting.

2. Instrument and Measurement Concept

The GIFTS uses large area format focal plane array (LFPA) infrared (IR) detectors (128 × 128) in a Fourier Transform Spectrometer (FTS) mounted on a geosynchronous satellite to gather high-spectral resolution (0.6 cm^{-1}) and high-spatial resolution (4-km footprint) Earth infrared radiance spectra over a large geographical area (512-km × 512-km) of the Earth within a 10-second time interval. A low light level visible camera provides quasi-continuous imaging of clouds and surface at 1-km footprint spatial resolution. Extended Earth coverage is achieved by step scanning the instrument field of view in a contiguous fashion across any desired portion of the visible Earth. The radiance spectra observed at each time step are transformed to high vertical resolution (1-2 km) temperature and water vapor mixing ratio profiles using rapid profile retrieval algorithms. These profiles are obtained on a 4-km grid and then converted to relative humidity profiles. Images of the horizontal distribution of relative humidity for atmospheric levels, vertically separated by approximately 2 km, will be constructed for each spatial scan. The sampling period will range from minutes to an hour, depending upon spectral resolution and area coverage selected for the measurement. Successive images of clouds and the relative humidity for each atmospheric level are then animated to reveal the motion of small-scale thermodynamic features of the atmosphere, providing a measure of the wind velocity distribution as a function of altitude. The net result is a dense grid of temperature, moisture, and wind profiles which can be used for atmospheric analyses and operational weather prediction. O_3 and CO features observed in their spectral radiance signatures provide a measure of the transport of these pollutant and greenhouse gases. It is the unique combination of the Fourier transform spectrometer and

the large area format detector array (i.e., an imaging interferometer), and the geosynchronous satellite platform, that enables the revolutionary wind profile and trace gas transport remote sensing measurements. The imaging FTS produces the interferometric patterns for spectral separation of scene radiation reaching the detector arrays. To limit the background signal, the FTS is cooled by the first stage of a cryocooler to <150 K, while the detector arrays are cooled to <60K to maximize sensitivity. The high data rates generated by the focal plane arrays (FPAs) are reduced by loss-less data compression techniques and then passed to the telemetry system by low-power, low-volume, and next-generation electronic components. GIFTS will view areas of the Earth with a linear dimension of about 500-km, anywhere on the visible disk, for a period between 0.125 and 11.0 sec, depending on the data application (i.e., imaging or sounding). GIFTS uses two detector arrays within a Michelson interferometer to cover the spectral bands, 685 to 1130 cm^{-1} and 1650 to 2250 cm^{-1}, and achieve a wide range of spectral resolutions. These spectral characteristics are optimized to achieve all technological/scientific validation objectives of GIFTS, as well as the sounding accuracy desired for a future operational sounding system. The Michelson interferometer, or FTS, approach for geosyncronous satellite applications allows spectral resolution to be easily traded for greater area coverage or higher temporal resolution. The 4-km footprint size of the IR LFPAs enable sounding to the ground, under most broken-to-scattered cloud situations, and resolving small scale atmospheric water vapor and cloud features required for wind profiling.

3. AIRS and NAST-I

AIRS. The AIRS instrument is the first spaceborne spectrometer designed to meet the 1-K/1-km sounding accuracy objective by measuring the infrared spectrum quasi-continuously from 3.7 to 15.4 microns with high spectral resolution ($v/\delta v = 1200/1$). The sensitivity requirements, expressed as Noise Equivalent Differential Temperature (NEdT), referred to a 250-K target-temperature ranges, from 0.1 K in the 4.2-μm lower tropospheric sounding wavelengths to 0.5 K in the 15-μm upper tropospheric and stratospheric sounding spectral region. Table 1, below, summarizes the AIRS measurement characteristics. The AIRS Instrument provides spectral coverage in the 3.74 μm to 4.61 μm, 6.20 μm to 8.22 μm, and 8.8 μm to 15.4 μm infrared wavebands at a nominal spectral resolution of $v/\delta v = 1200$, with 2378 IR spectral samples and four visible/near-infrared (VIS/NIR) channels between 0.41 and 0.94 microns. Spatial

coverage and views of cold space and hot calibration targets are provided by a 360-degree rotation of the scan mirror every 2.67 seconds

Table 1. AIRS Measurement Characteristics

Data Rate	1.27 Mbits per second
Spectral Range	IR: 3.74 – 15.4 microns VIS/NIR: 0.4 – 1.1 microns
Instrument Field of View	IR: 1.1 degree (13.5 km at nadir from 705 km altitude) VIS/NIR: 0.2 degree (2.3 km from 705 km altitude)
Swath Width	99 degree (1650 km from 705 km orbit altitude)
Scan Sampling	IR: 90 x 1 x 1.1 degree VIS/NIR: 720 x 8 x 0.2 degree

NAST-I. The National Polar-orbiting Operational Environmental Satellite System (NPOESS) Airborne Sounding Testbed-Interferometer (NAST-I) was developed by the NPOESS Integrated Program Office (IPO) to be flown on high altitude aircraft and provide experimental observations especially needed for finalizing specifications and testing proposed designs and data processing algorithms for the Cross-track Infrared Sounder (CrIS) which will fly on NPOESS. As shown in Figure 1, the NAST-I has a spectral range of 3.6–16.1 μm, without gaps, and covers the spectral ranges and resolutions of all current and planned advanced high spectral resolution infrared spectrometers to fly on polar orbiting and geostationary weather satellites, including the EOS-AIRS, METOP-IASI (Infrared Atmospheric Sounding Interferometer), the NPP (NPOESS Preparatory Project)/NPOESS-CrIS (Cross-track Infrared Sounder), and the EO-3/GIFTS. The NAST-I spectral resolution is equal to, in the case of IASI, or higher than all current and planned advanced sounding instruments. Thus, the NAST-I data can be used to simulate the radiometric observations to be achieved from these advanced sounding instruments. Moreover, the forward radiative transfer models and product retrieval algorithms planned for these satellite systems can be validated prior to launch. Finally, NAST-I can be used for the fundamental purpose of post-launch calibration and validation of sensors and data products for the advanced satellite sounding systems. The NAST-I spatially scans the Earth and atmosphere from an aircraft, such as the high-altitude NASA ER-2 research airplane or the Northrop-Grumman Proteus aircraft. From an aircraft altitude of 20 km, 2.6 km spatial resolution is achieved, thereby providing three-dimensional hyperspectral images of radiance and derived geophysical products.
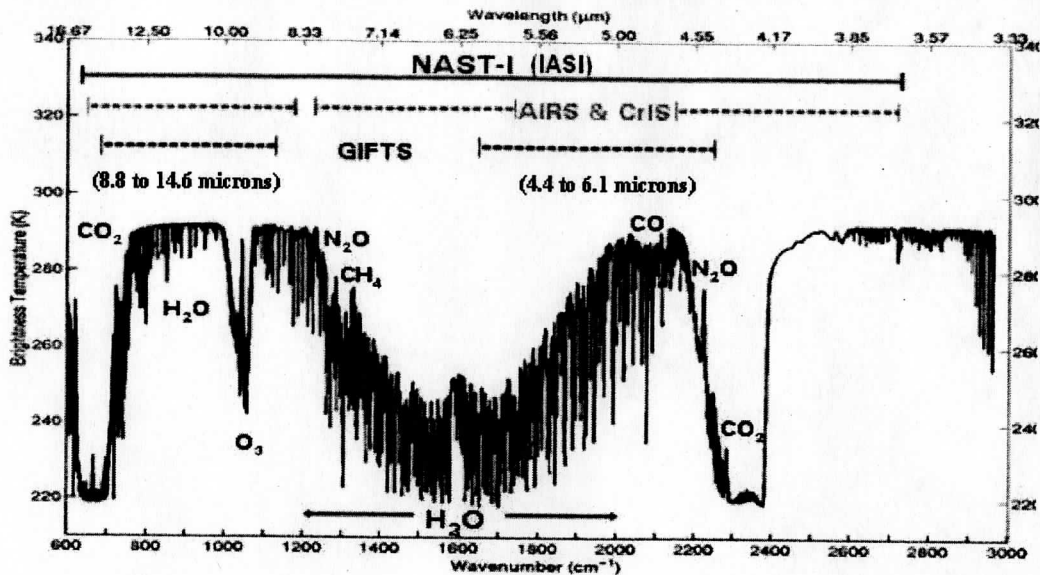
Figure 1. The NAST-I spectral coverage compared to that of advanced satellite sounders.

NAST-I provides a vertical resolution of 1–2 kilometers for atmospheric temperature and water vapor, so that distinct number of layers observed depends upon aircraft altitude. As the aircraft passes over the Earth, NAST-I scans an area at the Earth's surface collecting data on the properties of the Earth's surface and atmosphere beneath the aircraft. These data provide a wide variety of surface and atmospheric sounding and cloud products in support of scientific studies as well as provide a means to validate radiative transfer models and inverse algorithms to be used with sounding instruments, such as the EOS AIRS, NPOESS CrIS, and the NMP GIFTS.

4. Retrieval Approach and Accuracy

Temperature and moisture sounding capability of a high spectral resolution infrared sounder, such as the GIFTS, has been assessed with the Aqua satellite AIRS spectrometer and the NAST-I interferometer sounder during several field campaigns. The retrieval results to be shown were obtained using the eigenvector regression retrieval method as applied to high-spectral resolution radiance data. In this technique, a training sample of historical radiosonde data is used to simulate radiance spectra for the NAST-I instrument. In the simulation, the radiosonde temperature and humidity structure is used to diagnose the cloud top level. For the spectral radiance calculations, each radiosonde, which possesses a cloud, is treated as both a clear sky and as an opaque cloud condition profile. The opaque sky condition profile is created by representing the radiosonde temperature

and moisture profile below the cloud as isothermal, at the cloud top temperature, and as saturated. This profile adjustment enables the retrieval system to obtain a clear sky equivalent temperature and moisture profile, from a radiative transfer point of view, regardless of the cloud condition. If the sky is cloud free, then the correct atmospheric profile will be obtained from aircraft level down to the Earth's surface. If an opaque cloud exists, the correct atmospheric profiles will be retrieved down to cloud top with a saturated isothermal profile, at cloud top temperature, being retrieved below the cloud top down to the Earth's surface. If a semi-transparent or broken cloud cover exists, then the correct profile will be retrieved down to the cloud top level with a less than saturated moisture profile and a temperature profile intermediate to the true profile and the cloud top temperature, being retrieved below the cloud, the proportion of isothermal and saturation being dependent on the cloud opacity and fractional coverage. The surface emissivity spectrum for each radiosonde profile is randomly selected from a set of laboratory measured emissivity spectra for a wide variety of surface types. Trace gas species, such as ozone and carbon monoxide, were specified using a statistical representation based on correlations of these gases with temperature and humidity conditions specified by the radiosonde data.

Radiance eigenvectors are computed and regressions equations are derived which relate the radiosonde temperature and water vapor values to the radiance eigenvector amplitudes. The regression coefficients are determined for different numbers of eigenvectors used to represent the radiance spectra. The appropriate number of eigenvectors to be used for the retrieval is determined from a small representative spatial sample of radiance observations. The optimum number of eigenvectors for the retrieval is defined as that number which minimizes the spatial RMS difference between the radiance spectra calculated from the retrievals and the observed radiance spectra from which those retrievals were produced. This number generally ranges between 15 and 50, depending upon the variance associated with the particular data set used (higher natural variance requires a larger number of eigenvectors to represent the information content of the radiance spectra). The regression equations for the "optimal" number of radiance eigenvectors are then applied to the spectral radiance measurements for the entire spatial domain and time period being analyzed. Since the radiative transfer calculations and

eigenvector decomposition analysis are done "off-line", the routine retrieval production is extremely fast.

Both theoretical and experimental validations indicate that the AIRS and NAST-I temperature and water vapor profiles, for clear air conditions (i.e., clear atmospheric columns or above clouds), have an accuracy near 1 K, for the atmospheric temperature, and <15 %, for atmospheric relative humidity, when averaged over 1 km thick vertical layers.

5. Example Results

Figure 2 below shows a vertical cross section of AIRS and NAST-I relative humidity retrievals for 26 July 2002 off the east coast of Florida during an Aqua satellite overpass of the Proteus aircraft flight track.
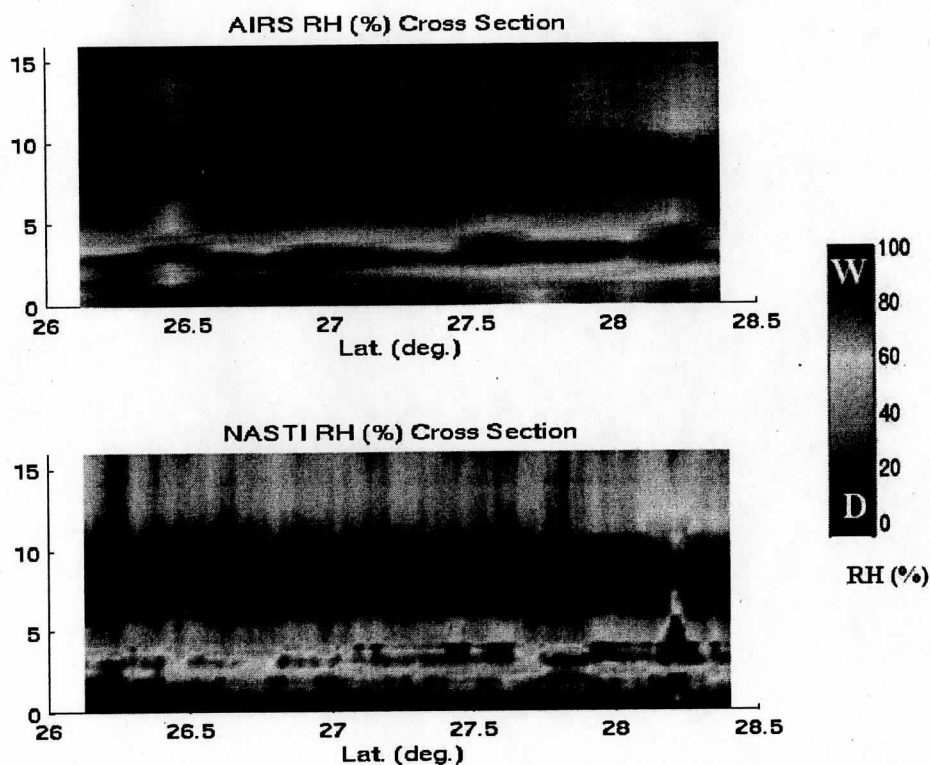
Figure 2: Comparisons between vertical cross sections of atmospheric relative humidity retrieved from AIRS and NAST-I radiance spectra. "W" and "D" denote Wet and Dry values.

Small scale differences in the water vapor cross sections can be seen as a result of the spectral and spatial resolution differences between the two instruments. The difference in the sensitivity to the water vapor above the 10 km level is due to the large difference between the spectral resolution for the two instruments (i.e., ~1.25 cm^{-1} for AIRS vs 0.25 cm^{-1} for NAST) which causes a difference in their abilities resolve emission

contributions, which originate from the high troposphere, from the centers of strong water vapor absorption lines.

Figure 3 shows a comparison of a cross section of atmospheric temperature, deviation from its level mean value, as retrieved from Aqua satellite AIRS and NAST-I radiances, observed from the ER-2 aircraft at the 20 km level, on March 3, 2003 near Hawaii. As can be seen, the fine scale vertical temperature profile features retrieved from the AIRS and NAST-I radiance data
compare well with data from dropsondes released from the NOAA G-4 aircraft at an altitude of 13 km. (Note that for this illustration the NAST-I spatial resolution has been reduced to that of AIRS, i.e., 15 km, and that the AIRS retrievals were produced from 3 x 3 averages of spectra about their central nadir positions in order to minimize the effects of measurement noise on the retrieval of fine scale vertical temperature structure.) The vertical resolution difference in the temperature reversal feature in the 9-10 km layer is expected due to the lower vertical resolution of the retrievals compared to the in-situ dropsonde measurements. The satellite and aircraft retrieval cross-section shows somewhat higher horizontal resolution features than inherent in the dropsonde cross section because they are derived from ten relatively closely spaced (~15 km) retrievals, whereas the dropsonde cross-section is based on only three profiles (with about a 75 km separation distance), one at each end, and one in the middle, of the cross section shown in Figure 3. It is particularly noteworthy that the cross section mean of the AIRS and NAST-I profiles is almost identical to the mean of the dropsonde observations.
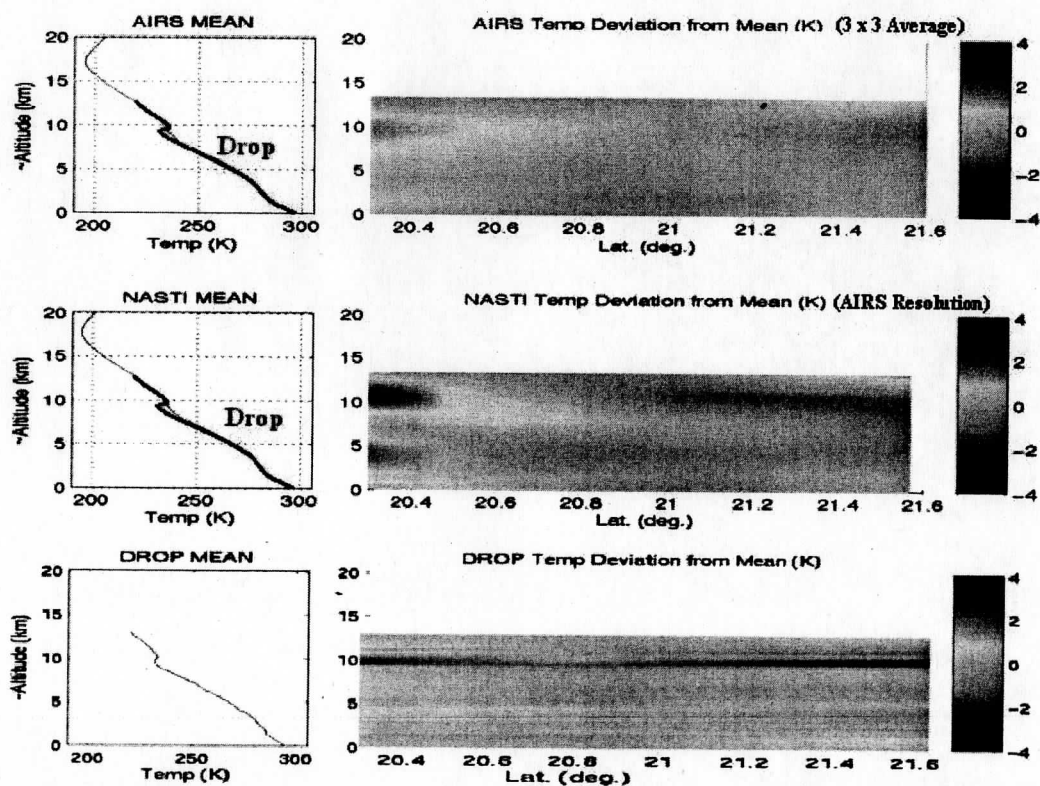

Figure 3. Comparison between cross sections of temperature (deviation from the level mean value) for AIRS and NAST retrievals, at AIRS spatial resolution, and dropsonde

observations near Hawaii on March 3, 2003. Red and Blue areas are relatively warm and cold areas, respectively.

6. Summary

GIFTS hyperspectral instrument will provide high spatial and temporal resolution temperature and moisture soundings from geosynchronous orbit from which wind profiles can be determined. The initial sounding retrieval technique to be applied to GIFTS data has been demonstrated and validated through its application to polar orbiting satellite AIRS spectrometer and high altitude aircraft NAST interferometer sounding radiance spectra. Full exploitation of the GIFTS will rely on the assimilation of its continuous data stream in numerical weather prediction models.

7. Bibliography

H. Aumann et al. , "AIRS Level 1b Algorithm Theoretical Basis Document (ATBD) Part 1 (IR),"., December 15, 1999

W. L. Smith, H. E. Revercomb, and G. E. Bingham, "Geostationary Fourier Transform Spectrometer (GIFTS) – The New Millennium Earth Observing-3 Mission", *Proc. of IRS 2000: Current Problems in Atmospheric Radiation*, A Deepak Publishing, Hampton, Virginia, 2001.

W. L. Smith, A. M. Larar, D. K. Zhou, C. A. Sisko, J. Li, B. Huang, H. B. Howell, H. E. Revercomb, D. Cousins, M. J. Gazarik, D. Mooney, "NAST-I: results from revolutionary aircraft sounding spectrometer", *SPIE Optical Spectroscopic Techniques and Instrumentation for Atmospheric and Space Research III*, A. M. Larar, Ed., 3756, 2–8, 1999.

D. K, Zhou, W. L. Smith, J. Li, H. B. Howell, G. W. Cantwell, A. M. Larar, R. O. Knuteson, D. C. Tobin, H. E. Revercomb, and S. A. Mango, "Thermodynamic product retrieval methodology for NAST-I and validation," *Applied Optics*, 41, 6,957–6,967, 2002.

Extraction of Profile Information from Cloud Contaminated Radiances

W. L. Smith, D. K. Zhou[1], H-L Huang[2], Jun Li[2], X. Liu[1], and A. M. Larar[1]

[1] NASA Langley Research Center, Hampton VA
[2] UW-CIMSS, Madison WI
bill.l.smith@cox.net

1. Introduction

Clouds act to reduce the signal level and may produce noise dependence on the complexity of the cloud properties and the manner in which they are treated in the profile retrieval process. There are essentially three ways to extract profile information from cloud contaminated radiances: (1) cloud-clearing using spatially adjacent cloud contaminated radiance measurements, (2) retrieval based upon the assumption of opaque cloud conditions, and (3) retrieval or radiance assimilation using a physically correct cloud radiative transfer model which accounts for the absorption and scattering of the radiance observed. Cloud clearing extracts the radiance arising from the clear air portion of partly clouded fields of view permitting soundings to the surface or the assimilation of radiances as in the clear field of view case. However, the accuracy of the clear air radiance signal depends upon the cloud height and optical property uniformity across the two fields of view used in the cloud clearing process. The assumption of opaque clouds within the field of view permits relatively accurate profiles to be retrieved down to near cloud top levels, the accuracy near the cloud top level being dependent upon the actual microphysical properties of the cloud. The use of a physically correct cloud radiative transfer model enables accurate retrievals down to cloud top levels and below semi-transparent cloud layers (e.g., cirrus). It should also be possible to assimilate cloudy radiances directly into the model given a physically correct cloud radiative transfer model using geometric and microphysical cloud parameters retrieved from the radiance spectra as initial cloud variables in the radiance assimilation process. This presentation reviews the above three ways to extract profile information from cloud-contaminated radiances. NPOESS Airborne Sounder Testbed-Interferometer (Smith et. al., 1999) radiance spectra and Aqua satellite AIRS (Aumann et. al., 2003) radiance spectra are used to illustrate how cloudy radiances can be used in the profile retrieval process.

2. Cloud Handling Techniques

The vertical resolution of soundings obtained from high spectral resolution infrared spectrometers is highly dependent on the radiance signal to noise ratio. Clouds act to reduce the signal level and may produce noise dependent on the complexity of the cloud properties and the manner in which they are treated in the profile retrieval process. There are essentially four ways used to deal with clouds: (a) hole hunting, (b) cloud-clearing using spatially adjacent radiance measurements, (c) opaque cloud training, and (d) realistic cloud training.

(a) Hole hunting: The success of hole hunting is highly dependent upon the instrument field of view size. Figure 1 below shows that for the field of view size of the current and planned polar orbiting sounding instruments (i.e., AIRS, IASI, and CrIS), the percentage of 50 km x 50 km sounding regions with clear fields of view will be too small (i.e., < 30 %) to provide adequate global sounding coverage. Thus, we must be able to treat clouds in either the sounding retrieval or the radiance assimilation process in order to get the full value of these data in global numerical weather prediction.
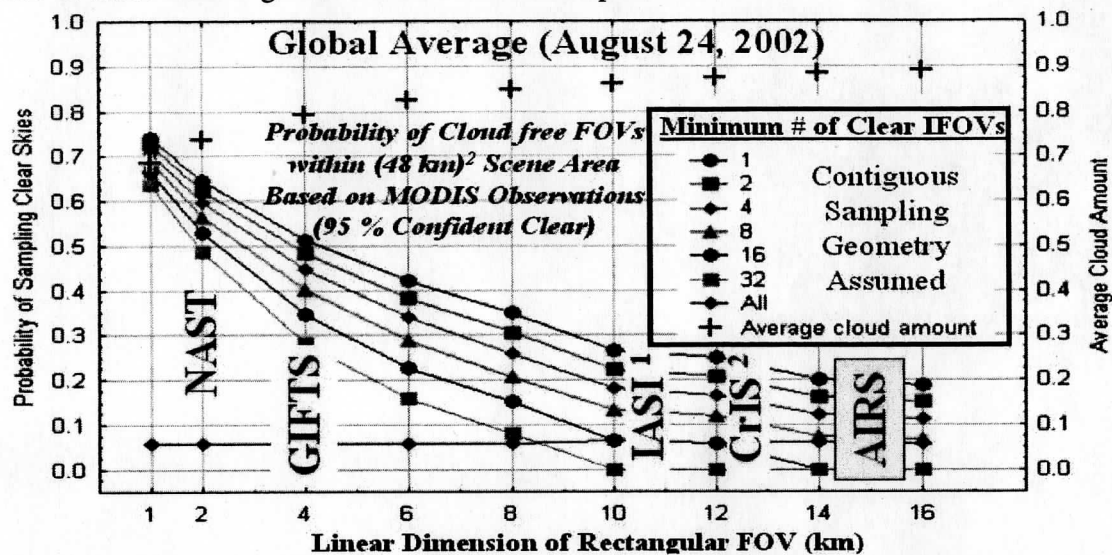
¹IASI is circular with a diameter of 12 km, ² CrIS is circular with a diameter of 14 km

Figure 1: Probability of sampling clear air as a function of field of view size

(b) Cloud clearing: Cloud clearing produces the radiance observed in the clear air portion of a partly cloudy area, and therefore soundings to the surface, when the cloud height and optical properties are horizontally uniform (Smith, 1968). Figure 2 below shows a cloud-clearing algorithm formulated for utilizing high spatial resolution imager observations (i.e., MODIS) for processing the low spectral resolution Aqua AIRS spectral radiance data. As can be seen, under the assumption of horizontally uniform surface and atmospheric condition, including cloud height and cloud microphysical properties, the radiance for the clear portion of a set of partly cloudy fields of view can be extracted from the cloud contaminated radiances given a single parameter, N^*. Since N^* is independent of spectral frequency, it can be defined from the observed radiances for a single spectral channel whose radiance is heavily influenced by the cloud, provided that the clear radiance for that channel is known. N^* can thus be defined by using the clear air radiances observed within the two adjacent sounding instrument fields of view as observed with a high spatial resolution imager together with the cloud contaminated radiances observed with the sounding instrument. In this case the radiances for an atmospheric window spectral region (i.e., 10.5 – 11.5 micron) are used for both instruments. The high spectral resolution radiances from the sounding instrument are spectrally convoluted using the instrument response function of the lower spectral, but higher spatial, resolution imaging radiometer for the determination of N^*. Once N^* is defined, the clear air spectrum for the sounding instrument can be calculated as shown in

figure 2. Other imager instrument clear air spectral channel radiances can then be approximated by spectral convolutions of the derived sounder clear air spectrum. A comparison of the sounder simulated clear air radiances for the imaging instrument spectral channels with those actually observed by the imager enables erroneous estimates arising from non-uniform surface and atmospheric conditions to be filtered from the set to be used for atmospheric sounding determination or for direct assimilation into the NWP model analysis/prediction process.
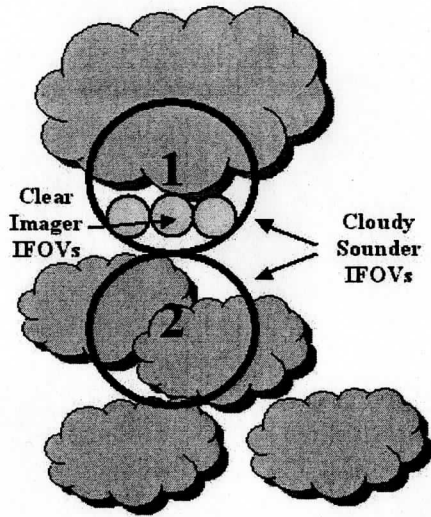
$$R_{clr}(v) = \frac{R_1(v) - N^*(v)R_2(v)}{1 - N^*(v)}$$

where $N^*(v) = \varepsilon(v)_1 N_1 / \varepsilon_2(v) N_2$.

$$N^*(W) = \frac{R_1(W) - \overline{R_{clr}}(\Delta W)}{R_2(W) - \overline{R_{clr}}(\Delta W)}$$

$$\hat{R}_{clr}(\Delta v) = \int \theta(v) R_{clr}(v) dv$$

Filter:

$$\left| \hat{R}_{clr}(\Delta v) - R_{clr}(\Delta v) \right| \geq \delta$$

$R_1(W)$ and $R_2(W)$ are sounder window radiance measurements in FOVs 1 and 2. $R_{clr}(\Delta W)$ is the clear window radiance measured by the imager. $R_{clr}(\Delta v)$ is the clear radiance measured in the absorption channel(s) of the imager. δ is the expected error, due to measurement noise, between the true and reconstructed imager clear radiances.

Figure 2: Basic cloud clearing methodology. The relationships are valid under the assumption of horizontally uniform cloud height and microphysical properties.

For the case of the Aqua satellite, the MODIS imaging spectrometer possesses numerous 1 km spatial resolution spectral absorption channels, which overlap the spectral coverage of the AIRS (see figure 3 below).
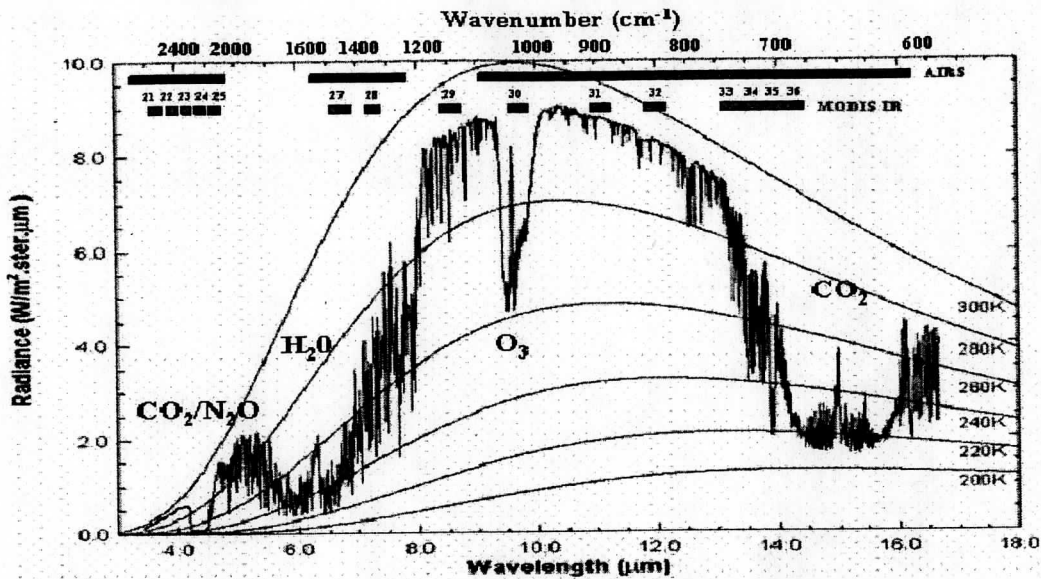
Figure 3: MODIS spectral channels (green) and AIRS spectral coverage (red).

An example of the extraction of the clear air radiance from a set of cloud-contaminated fields of view is shown in figure 4. Here the derived clear air spectrum is compared with a nearby observed clear sky spectrum. The derivation is for radiances observed over water and for low-level scattered cumulus cloud conditions. As can be seen, the clear air spectrum is successfully determined for this case.
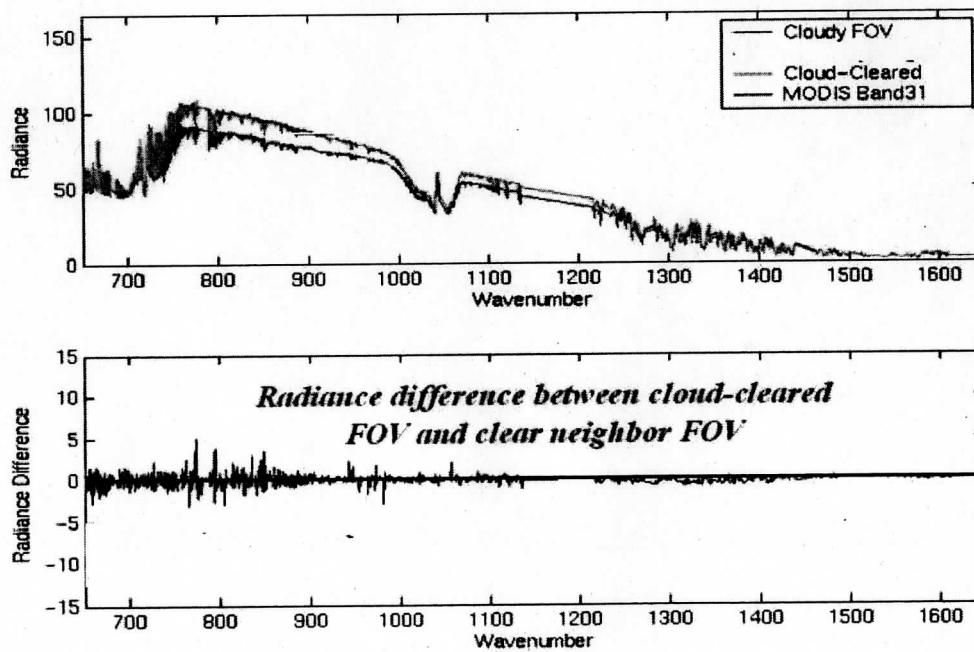

Figure 4: Example clear air radiance spectrum derived from the combination of Aqua AIRS and MODIS data

Table 1 below shows the clear air sounding radiance yields without and with the use of MODIS absorption channel data for filtering erroneous cloud cleared radiance spectra.

Here, the radiance spectra, for different spatial resolutions, and MODIS observations were simulated from NPOESS Airborne Sounder Testbed Interferometer (NAST-I) data, which have a 3 km spatial resolution (Smith et. al., 2003). Only cases where at least one clear NAST-I field of view within the 40 km x 40 km sounding area were included in the analysis since for these cases the correct clear radiance spectrum was known for validation purposes. The spatial resolution most representative of the AIRS is the 18 km linear resolution case. As shown, the yields of the MODIS absorption channel filtered data are only slightly lower than the unfiltered data indicating that the high N* filter (**i.e.,** **N* > 0.75**) was able to detect many of the erroneous cloud cleared radiance estimates.

Table 1: 40 km x 40 km Sounding Area Clear Field of View Radiance Yields (%)

Spatial Resolution	3km	6km	9km	12 km	18 km
Total Number of FOVs/ FOR	144	36	16	9	4
≥ 1 Observed Clear FOV/FOR (%)	46	40	33	28	21
Total (Clr + CCR) w/o MODIS (%)	66	62	56	53	45
Total with MODIS (%)	**64**	**58**	**52**	**47**	**39**

However, as shown in figure 5 below, there is a significant difference in the accuracy between the error estimates for these two cases. Without the use of the MODIS filter, the errors of the clear sky estimates are too large to be useful for retrieval or radiance assimilation. With the use of MODIS, more acceptable results are achieved but these errors are still larger than those desired for the extraction of profile information with high vertical resolution.
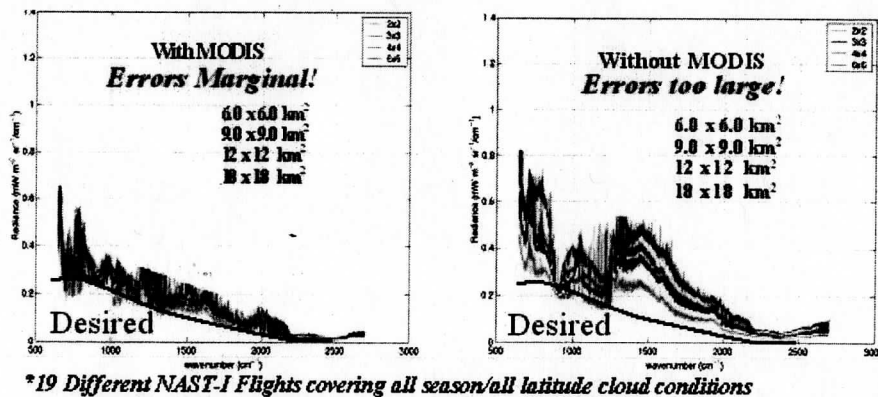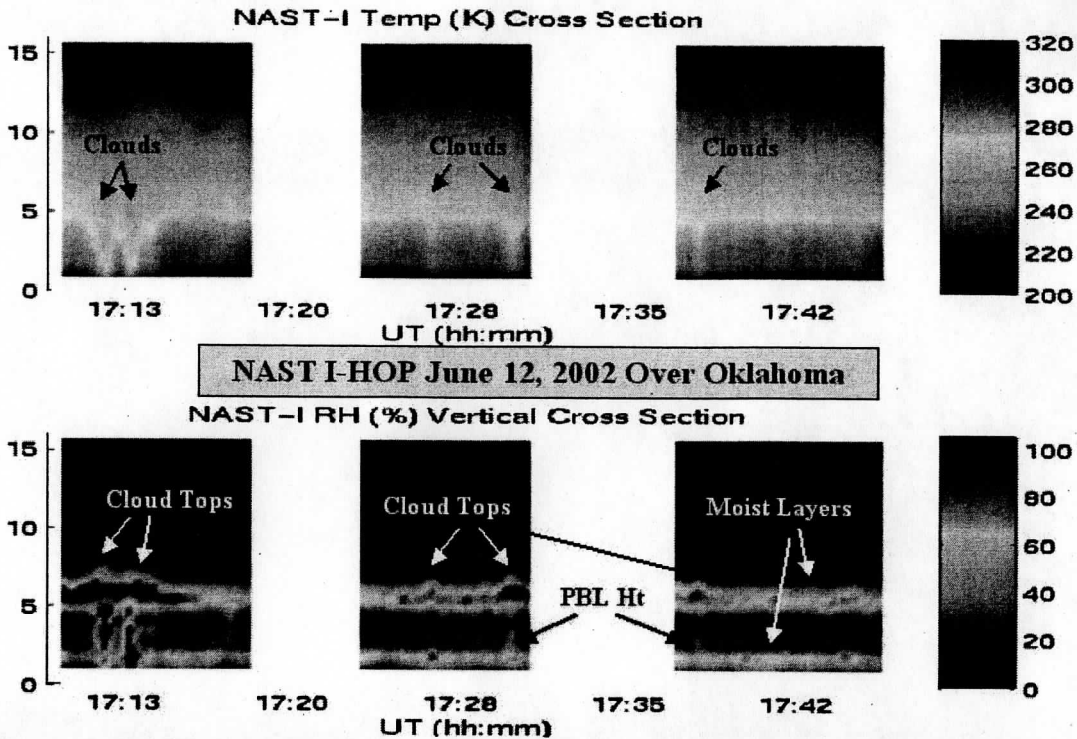

*19 Different NAST-I Flights covering all season/all latitude cloud conditions

Figure 5: Cloud clearing with and without imager absorption channels (i.e., MODIS).

(c) Opaque cloud assumption: Assuming that opaque clouds exist within the instruments field of view produces, accurate profiles can be retrieved down to levels

close to the cloud top level. This is because there is an ambiguity between an opaque cloud condition and a clear atmospheric profile, which is isothermal below the cloud level. The vertical resolution of the hyperspectral radiance measurements is high enough to resolve the equivalent isothermal condition within 1-2 km of the cloud level. Thus merely treating an opaque cloud radiance spectrum as if it were from a clear sky atmospheric condition should tend to result in the retrieval of the correct atmospheric profile above the cloud top level, with a fictitious isothermal, and saturated, profile condition being retrieved below the cloud top level. The retrieved relative humidity and the abrupt change in vertical temperature lapse rate enable one to determine the cloud level.

Figure 6 below shows an example of results assuming clear atmospheric conditions for cloud-contaminated radiances as observed with the NAST-I instrument. Here the retrieval method is the Eigenvector (EOF) regression method (Smith and Woolf, 1976, and Zhou et. al., 2002) where training data set, used for the radiative transfer calculations, included cloudy radiosondes in which the temperature profile was adjusted to be isothermal, and the relative humidity was set to 100 %, below the cloud level (Smith et al., 2004). Thus, the regression relations were trained to retrieve the clear sky equivalent profiles below the cloud under cloudy sky conditions. As can be seen, under the clear sky assumption, the temperature tends toward the isothermal condition and the relative humidity tends toward saturation to a degree dependent upon the opacity of the cloud. Even in the clear air columns between the cloud elements, where the temperature profile does not tend towards the isothermal condition, the layer of high moisture responsible for the existence of the nearby clouds can be seen in the relative humidity vertical structure. The advantage of this simple approach for handling clouds is that it allows profile information down to cloud level to be assimilated into the model. However, it is not clear how to incorporate this information for the case where one is assimilating radiances rather than retrievals. One method might be to replace the erroneous profile retrieved below the cloud top level with the model profile and recompute the radiances using the hybrid profiles. The radiances whose weighting functions peak at and above the cloud level, which are heavily influenced by the retrieved profiles above cloud level, can then be assimilated as clear air radiances.

NAST-I Temp (K) Cross Section

NAST I-HOP June 12, 2002 Over Oklahoma

NAST-I RH (%) Vertical Cross Section

Figure 6: NAST-I retrieved temperature and moisture structure for a broken cloud condition with cloud tops near the 6 km level.

(d) Realistic Cloud Radiative Transfer Model: However, if the clouds are high and there is significant spectral structure in the absorption of the clouds (i.e., a common characteristic of Cirrus clouds), errors in the profiles above the clouds may occur. Thus for high cloud cases, a more realistic cloud model is required to get accurate profiles down to the cloud top level. Also, if the cloud is semi-transparent or broken, the profile below the cloud level should be retrievable using a physically based cloud radiative transfer model. The physically based cloud radiative transfer model was developed by the University of Wisconsin – CIMSS (Huang et. al., 2004) using DISORT calculations performed for a wide variety of cloud microphysical properties by Ping Yang, at the Texas A&M University (Yang et. al., 2003). For the retrieval using the EOF regression method, the clouds can now be included in a more realistic manner with a statistical distribution in accordance with real observations conducted over many years from aircraft and balloon (Heymsfeld et al., 2003). Table 2 below summarizes the characteristics of the realistic cloud model and the simulations of clouds as used for the EOF regression training. For semitransparent and/or scattered cloud with an effective optical depth (defined here as the exponential of a negative argument which is the product of the fractional cloud amount times the cloud visible optical depth), which is less than unity, the correct profile below the cloud is attempted to be retrieved. If a lower level cloud underlies the semitransparent and/or scattered upper level cloud, the lower level cloud is treated as an equivalent clear isothermal condition as described above for the opaque cloud condition retrieval. EOF regression enables both the cloud height and the cloud microphysical properties of the highest-level cloud to be estimated.

## Table 2: Cloud Radiative Transfer Model and Cloud Simulation Characteristics

- **Perform a realistic simulation of clouds for synthetic EOF radiance training**
- **Diagnose 0-2 cloud layers from radiosonde relative humidity profile**
    - A single cloud layer (either ice or liquid) is inserted into the input radiosonde profile.
    - Approximate lower level cloud using opaque cloud representation (i.e., isothermal/saturated)

- **Use parameterization of Heymsfeld's[*] balloon and aircraft cloud microphysical data base (2003) to specify cloud effective particle radius, r_e, and cloud optical depth, τ, (i.e., $r_e = a \tau^\alpha / [\tau - b\tau^\alpha]$).**
    - Different habitats can be specified (Hexagonal columns assumed here)
    - Different clouds microphysical properties are simulated for same radiosonde using random number generator to specify visible cloud optical depth within a pre-specified range. 10% random error added to parameterized effective radius to account for real data scatter.
- **Use LBLRTM/DISORT "lookup table" to specify cloud radiative properties**
    - Spectral transmittance and reflectance for ice and liquid clouds interpolated from multi-dimensional look-up table based on DISORT multiple scattering calculations for the (wavenumber range $500 - 2500$ cm^{-1}, zenith angle $0 - 80$ deg., Deff (Ice: $10 - 157$ um, Liquid: $2 - 100$ um), OD(vis) (Ice: $0.04 - 100$, Liquid $0.06 - 150$)

- **Compute EOFs and Regressions from cloudy radiance data base**
    - Regress cloud properties (p, τ, r_e) and surface and profile parameters against radiance EOFs
    - For small optical depth, output entire profile down to surface or lower opaque cloud level
    - For large upper level cloud optical depth, output profile above the upper cloud level

Heymsfield, A. J., S. Matrosov, and B. A. Baum: Ice water path-optical depth relationships for cirrus and precipitating cloud layers. *J. Appl. Meteor.* October 2003

Figure 7 shows a vertical cross section of temperature and moisture profiles retrieved from NASA ER-2 aircraft NAST-I data for a very cloudy situation. The retrieved cloud height is compared with that estimated from a nadir looking Cloud Physics LIDAR (CPL) on-board the ER-2 aircraft. The flight track is shown over visible and IR images from the GOES spacecraft. A comparison of a NAST-I profile at 19 GMT with the 00 GMT MHX radiosonde is also shown alongside cross-section near the radiosonde station. The retrievals were produced using the EOF regression method where a very large sample of radiosondes from a ten year period was used to simulate NAST radiances. Clouds were introduced at levels where the radiosonde humidity exceeded a threshold prescribed as a function of altitude. Cloud microphysical properties were assigned using a random number generator to define an optical depth between 0 and 4, from a uniform distribution of the logarithm of the optical depth, and the effective particle radius was defined using the relation provided in table 2 above which is based on many years of cloud microphysical property observations from balloon and aircraft. The particle radius is changed by a random amount selected from a guassian distribution of random numbers with a standard deviation of 10% in order to represent the scatter of real observations. If two or more cloud layers exist, the lower level clouds are represented as a the equivalent cloudfree isothermal temperature condition in the radiative transfer calculation. Thus the attempt is to retrieve profiles below optically thin upper level cloud only (e.g., thin Cirrus). Regression relations are also generated for predicting cloud height, visible optical depth, and particle diameter. Because the radiance is highly non-linear with respect to cloud height, statistics are formulated for one class of data which contains all cloud height conditions and eight other height classes for which the cloud height has been stratified to within 1 km of the mean for that class. The final cloud height class to be used for the retrievals is obtained by iteration beginning with the unclassified class to predict the initial cloud height stratification for the retrievals. Usually, the final cloud height class is defined within five iterations of the cloud height prediction process.

In the retrievals shown in figure 7, the profiles retrieved below clouds with a predicted optical depth greater than 1 were considered missing since their accuracy would be degraded from that achievable under cloudless sky conditions.
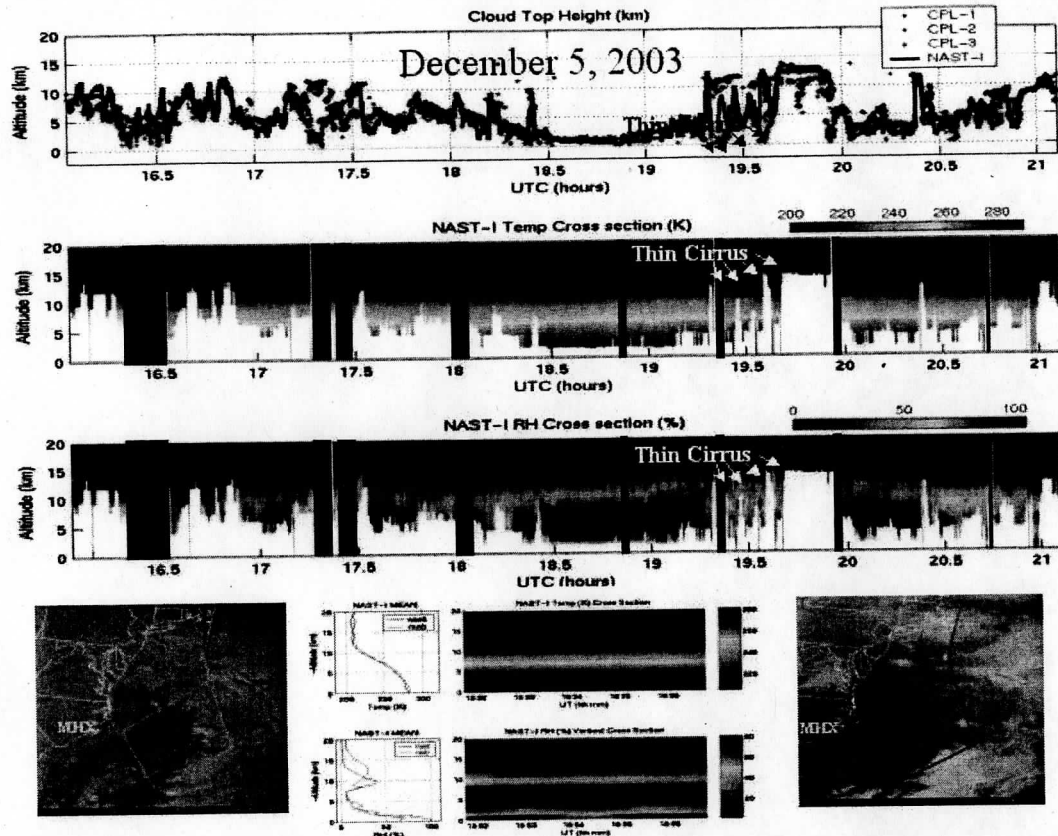
Figure 7: Temperature and humidity cross-sections from NAST-I cloud contaminated radiances observed along the flight track of the NASA ER-2 aircraft flying at 20km flight altitude over a wide variety of clouds.

As can be seen there is excellent agreement between the LIDAR and NAST-I retrieved cloud heights indicating that the retrieval of other properties, such as the cloud microphysical properties and the temperature and humidity profiles should also be accurate. The horizontal uniformity of the retrieved temperature and humidity conditions across the wide variety of cloud height conditions indicate that this is the case.

Evidence of the accuracy of the profile conditions which can be retrieved under cloud conditions is given by figure 8 which shows a comparison of the EOF regression retrievals for this case obtained from AIRS and NAST-I data in comparison to dropsonde observations made along the flight track of the ER-2. One can see excellent correspondence between all three observations even though their time differences may be as large as 4 hours.
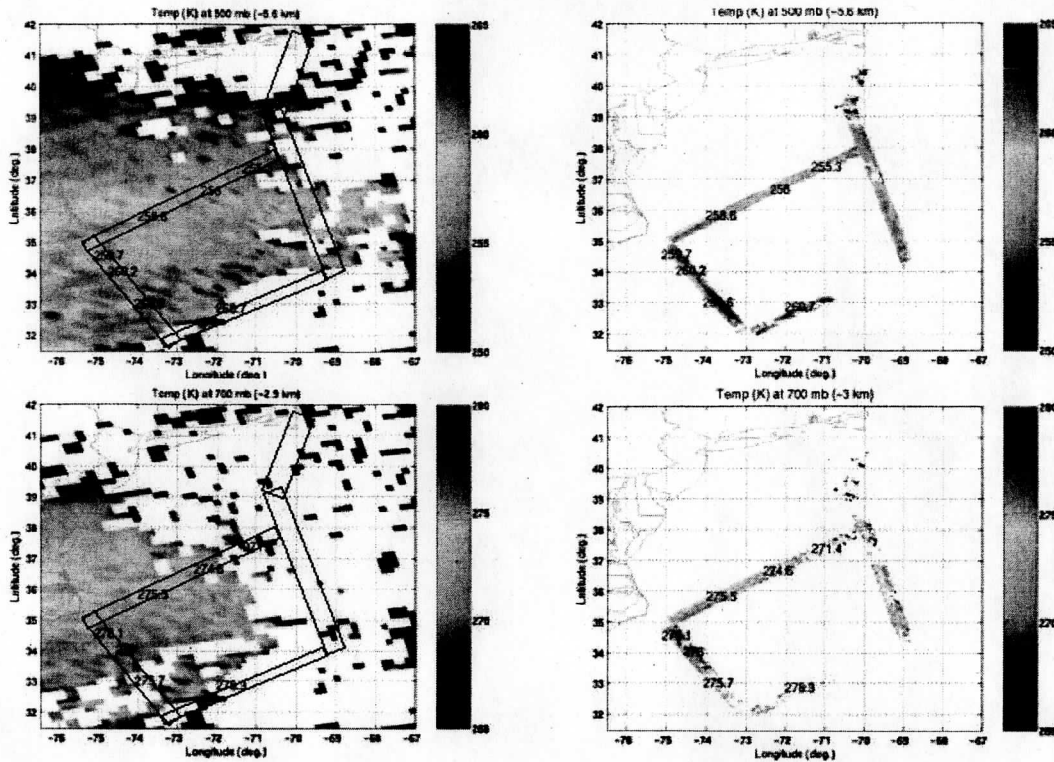
Figure 8: Retrievals of atmospheric temperature at 500mb and 700 MB obtained from Aqua satellite AIRS radiance spectra and NAST-I radiance spectra. Dropsondes from the NOAA Gulfstream along the track of the ER-2 aircraft are shown to validate the retrieval results.

For the radiance assimilation process, one might use the retrieved cloud height, optical depth, and particle diameter properties with the cloud radiative transfer model used here in the assimilation process. Spectral radiances for channels which peak below clouds with an optical depth greater than unity could be deleted from the assimilation process in order to minimize the effects of errors in the cloud representation.

3. Summary and Conclusions

Cloud greatly complicates the interpretation of infrared sounding data. The new hyperspectral resolution infrared sounding systems alleviate much of the ambiguity between cloud and atmospheric temperature and moisture contributions. However, in heavily clouded situations, the thermodynamic profile information to be retrieved is limited to the atmosphere above clouds. The results of the study presented here indicate some success in the ability to retrieve information below scattered and partially transparent Cirrus cloud (i.e., clouds with effective optical depths of less than unity). The thermodynamic profile information can be obtained by a combination of cloud clearing and by direct retrieval from the clouded radiances using a realistic cloud radiative transfer model. Results achieved with airborne NAST-I and Aqua satellite NAST-I observations show that accuracies close to those achieved in totally cloud-free conditions can be achieved down to cloud top levels. The accuracy of the profile retrieved below cloud top level is dependent upon the optical depth and fractional coverage of the cloud.

For the assimilation of cloudy radiances into an NWP model, two approaches might be considered: (1) an indirect method whereby clear sky equivalent radiances are assimilated, and (2) a direct method in which the actual cloud radiances are assimilated. For the indirect method, a combined EOF regression retrieval followed by a 1-d variational retrieval, using the cloud parameters from the EOF regression retrieval, is performed and the results above the highest cloud level with an effective optical depth greater than one is amalgamated with the model profile to recompute the equivalent clear sky radiances for the hybrid

atmospheric profile condition. One can then assimilate the "clear" radiance whose weighting functions peak above the derived cloud level.

In the direct cloudy radiance assimilation method, a cloudy sky condition radiative transfer model is used in the assimilation process. In this technique the intial cloud parameters for the radiative transfer calculation are taken from the EOF regression retrieval. The cloud parameters are allowed to adjust as part of the cloudy radiance assimilation process.

The implementation of either of the two approaches suggested above requires a considerable research development effort. However, cloudy sky radiative transfer models now exist which should enable the extraction of profile information from cloud contaminated radiances suitable for the numerical weather prediction application..

4. References

Aumann, Hartmut H.; Chahine, Moustafa T.; Gautier, Catherine; Goldberg, Mitchell D.; Kalnay, Eugenia; McMillin, Larry M.; Revercomb, Hank; Rosenkranz, Philip W.; Smith, William L.; Staelin, David H.; Strow, L. Larrabee, and Susskind, Joel. AIRS/AMSU/HSB on the Aqua Mission: Design, science objectives, data products, and processing systems. IEEE Transactions on Geoscience and Remote Sensing v.41, no.2, 2003, pp253-264.

Cousins, D., and W. L. Smith, 1997: National Polar-Orbiting Operational Environmental Satellite System (NPOESS) Airborne Sounder Testbed-Interferometer (NAST-I), in *Proceedings, SPIE Application of Lidar to Current Atmospheric Topics II*, A. J. Sedlacek, and K. W. Fischer, eds., 3127, 323–331.

Heymsfield, Andrew J.; Matrosov, Sergey, and Baum, Bryan. "Ice water path-optical depth relationship for cirrus and deep stratoform cirrus cloud layers". Journal of Applied Meteorology v.42 , no.10, 2003, pp1369-1390. Re

Huang, Hung-Lung; Tobin, Dave; Li, Jun; Olson, Erik; Baggett, Kevin; Huang, Bormin; Mecikalski, John; Knuteson, Bob; Osborne, Brian; Posselt, Derek; Antonelli, Paolo; Revercomb, Hank ; Smith, William, and Yang, Ping. "Hyperspectral radiance simulator - cloud radiance modeling and beyond". Optical Remote Sensing of the Atmosphere and Clouds III, Hangzhou, China, 25-27 October 2002. Bellingham, WA, International Society for Optical Engineering, (SPIE), 2003, pp180-189. Reprint #3477.

Liu, X., J.-L. Moncet, D. K. Zhou, and W. L. Smith, 2003: A Fast and Accurate Forward Model for NAST-I Instrument, *Fourier Transform Spectroscopy and Optical Remote Sensing of Atmosphere, OSA Topical Meetings*, Feb. 2003, Quebec, Canada.

Smith, W.L., 1968: And improved method for calculating tropospheric temperature and moisture from satellite radiometer measurements. *Mon. Wea. Rev.*, 96, 387-396.

Smith, W. L., and H. M. Woolf, 1976: The use of eigenvectors of statistical co-variance matrices for interpreting satellite sounding radiometer observations, *J. Atmos. Sci.*, 33, 1,127–1,140.

Smith, W. L., A. M. Larar, D. K. Zhou, C. A. Sisko, J. Li, B. Huang, H. B. Howell, H. E. Revercomb, D. Cousins, M. J. Gazarik, D. Mooney, 1999: NAST-I: results from revolutionary aircraft sounding spectrometer, in *Proceedings, SPIE Optical* A. M. Larar, ed., 3756, 2–8.

Smith, W. L., G. E. Bingham, G. W. Cantwell, M. J. Gordon, D. K. Zhou, and H-L. Huang, "AIRS Cloud-clearing Using Multi-spectral MODIS Imagery", Available from **bill.l.smith@larc.nasa.gov**

Smith, W. L., D. K. Zhou, A. M. Larar, S. A. Mango, H. B. Howell, R. O. Knuteson, H. E. Revercomb, and W. L. Smith Jr " The NPOESS Airborne Sounding Testbed Interferometer - Remotely Sensed Surface and Atmospheric Conditions during CLAMS", accepted fopr publication on the Journal of the Atmospheric Sciences, Special Issue: "Chesapeake Lighthouse and Aircraft Measurements for Satellites (CLAMS) Field Experiment", 2004

Yang P., B. C. Gao, B. A. Baum, Y. Hu, W. Wiscombe, S.-C. Tsay, D. M. Winker, S. L. Nasiri, 2001: Radiative Properties of cirrus clouds in the infrared (8-13 um) spectral region, *J. Quant. Spectros. Radiat. Transfer*, 70, 473-504.

Yang P., B.-C. Gao, W. Wiscombe, M. I. Mishchenko, S. Platnick, H.-L. Huang, B. A. Baum, Y. X. Hu, D. Winker, S.-C. Tsay, and S. K. Park, 2002: Inherent and apparent scattering properties of coated or uncoated spheres embedded in an absorbing host medium. Appl. Opt. 41, 2740-2759.

Yang, Ping; Wei, Heli; Kattawar, George W.; Hu, Yong X.; Winker, David M.; Hostetler, Chris A., and Baum, Bryan A. "Sensitivity of the backscattering Mueller matrix to particle shape and thermodynamic phase". Applied Optics v.42, no.21, 2003, pp4389-4395. Reprint #3557.

Zhou, D. K., W. L. Smith, J. Li, H. B. Howell, G. W. Cantwell, A. M. Larar, R. O. Knuteson, D. C. Tobin, H. E. Revercomb, and S. A. Mango, 2002: Thermodynamic product retrieval methodology for NAST-I and validation, *Applied Optics*, 41, 6,957–6,967.

Apperception of Clouds in AIRS Data

Hung-Lung Huang
Cooperative Institute for Meteorological Satellite Studies
Space Science and Engineering Center
University of Wisconsin-Madison
1225 West Dayton Street
Madison, WI 53705, USA
E-Mail: allenh@ssec.wisc.edu
and
William L. Smith
Center for Atmospheric Sciences
Hampton University
Hampton Virginia, 23668
E-Mail: bill.smith@hamptonu.edu

1. Introduction

Our capacity to simulate the radiative characteristics of the Earth system has advanced greatly over the past decade. However, new space based measurements show that idealized simulations might not adequately represent the complexity of nature. For example, AIRS simulated multi-layer cloud clearing research provides an excellent groundwork for early AIRS operational cloud clearing and atmospheric profile retrieval. However, it doesn't reflect the complicated reality of clouds over land and coastal areas. Thus far, operational AIRS/AMSU cloud clearing is not only of low yield but also of unsatisfying quality. This is not an argument for avoiding this challenging task, rather a powerful argument for exploring other synergistic approaches, and for adapting these strategies toward improving both indirect and direct use of cloudy infrared sounding data.

Ample evidence is shown in this paper that the indirect use of cloudy sounding data by way of cloud clearing is sub-optimal for data assimilation. Improvements are needed in quality control, retrieval yield, and overall cloud clearing retrieval performance. For example, cloud clearing over land, especially over the desert surface, has led to much degraded retrieval quality and often a very low yield of quality controlled cloud cleared radiances. If these indirect cloud cleared radiances are instead to be directly assimilated into NWP models, great caution must be used. Our limited and preliminary cloud clearing results from AIRS/AMSU (with the use of MODIS data) and an AIRS/MODIS synergistic approach have, however, shown that higher spatial resolution multispectral imagery data can provide much needed quality control of the AIRS/AMSU cloud clearing retrieval. When AIRS and MODIS are used synergistically, a higher spatial resolution over difficult terrain (especially desert areas) can be achieved and with a much improved accuracy. Preliminary statistical analyses of cloud cleared radiances derived from (1) operational AIRS/AMSU, (2) operational AIRS/AMSU plus the use of MODIS data as quality control, and (3) AIRS/MODIS synergistic single channel and two field of views cloud clearing are

presented. These results illustrate the strengths and weaknesses of the current AIRS/AMSU cloud clearing approach discussed above.

While major efforts and advances in sounding retrieval have been made with the AIRS/AMSU, and more recently with AIRS/MODIS cloud clearing retrieval, cloud clearing inadequacies remain and they are responsible for cloud artifacts in infrared measurements used to represent clear sky conditions within or near partly cloudy spatial domains. Cloud cleared radiances and their associated sounding profiles do not represent cloudy sky soundings nor should they be directly assimilated into numerical weather models without the necessary ancillary cloud information. Otherwise the model fields will be biased by clear sky conditions. Example ECMWF analysis and AIRS/AMSU cloud cleared retrieval profiles have demonstrated the above argument, specifically that AIRS/AMSU cloud cleared sounding profiles of both temperature and water vapor are distinctly different from the cloudy profiles exhibited in the ECMWF analyses. Global replacement of model profiles with cloud cleared radiances would bias the result toward cloud free conditions.

However, direct assimilation of cloudy sounding data may be feasible due to recent advances in fast and accurate forward radiative transfer models for the cloudy atmosphere. Although at an early stage of development, recent results indicate that successful cloud modeling will enable the direct assimilation of cloudy radiances in the near future.

2. Clouds in AIRS Data

Fig. 1 is a global composite of reflectance measurements made by the Moderate Resolution Imaging Spectro-radiometer (MODIS) (King et al. 1992) instrument on board the Aqua satellite. As can be seen at the MODIS imaging measurement sampling size (1 km Field of View (FOV) at nadir), clouds cover most of the earth.
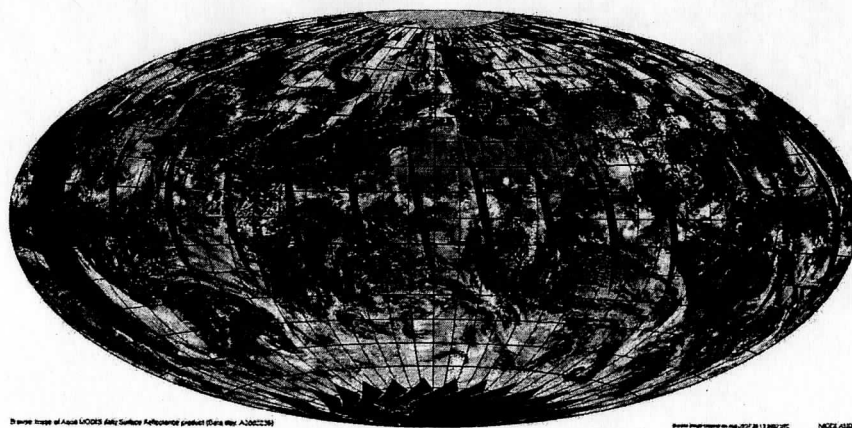
Fig. 1. Browse image of Aqua MODIS daily surface reflectance product showing cloud coverage.

For the Atmospheric Infrared Sounder (AIRS) (Aumann et al. 2003), which has nadir sampling FOV size greater than 14 km (depending upon scan angle), the impact of cloud cover is even greater. Some preliminary analyses have shown that only 5% of single AIRS FOVs are truly cloud free. The remaining 95% of AIRS data will require either cloud clearing, or an indirect

approach to physically account for the effects of clouds, or a direct approach that explicitly accounts for the influence of clouds via careful radiative transfer modeling. In the indirect approach, radiance or profile retrievals corrected for the presence of clouds are assimilated into Numerical Weather Prediction (NWP) models. In the direct approach, the cloud affected radiances themselves are assimilated. Fig. 2 shows examples of AIRS spectra showing the contrast between the clear and cloudy observations. Under clear and humid conditions (left column spectra of fig. 2), spectral features due to gaseous absorption of water vapor, carbon dioxide and ozone are very prominent. Spectral features due to solar reflectance, surface emissivity and reflectivity are not so obvious but are also embedded in the clear sky signal. Where clouds exist, they act as strong absorbers and reflectors as can be seen in the cloudy AIRS spectra (right column of fig. 2). As can be seen, clouds mask the clear sky and surface property spectral signal even when the scene is not fully covered by clouds. The cloud radiation portion of the radiance to space is a highly non-linear function of cloud altitude (single or multi-layer), phase (ice, water or mixed), and habit (particle size and shape). The relative differences between left and right spectra in fig. 2 can be viewed as important cloud forcing information for weather and climate prediction or a nuisance when attempting to use the cloud contaminated radiance data to retrieve atmospheric thermodynamic profile information for NWP applications. If cloudy scene radiance data are to be assimilated into NWP models, a physical radiative transfer model that accurately accounts for gaseous absorption and cloud forcing is needed.
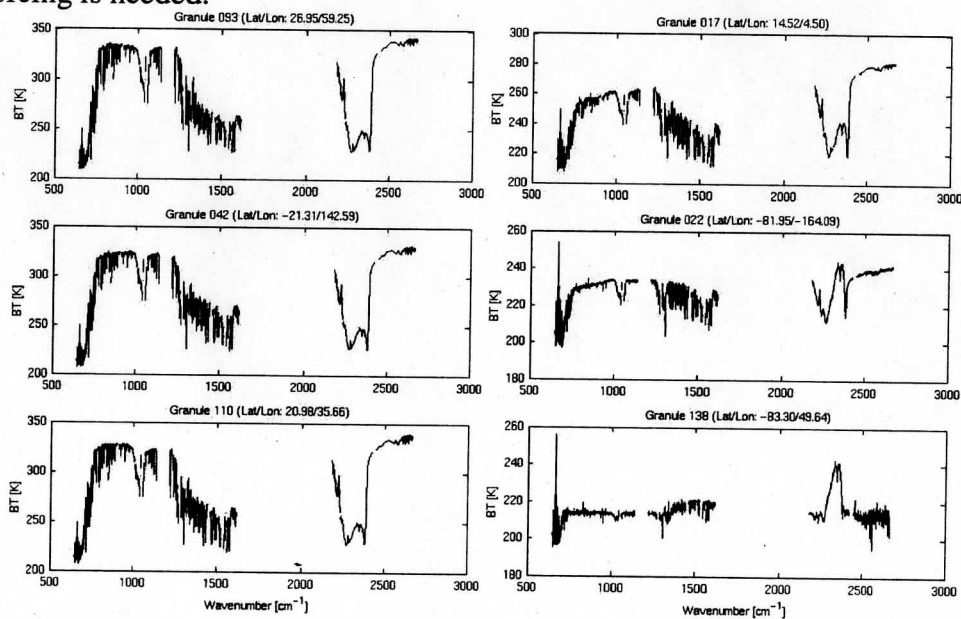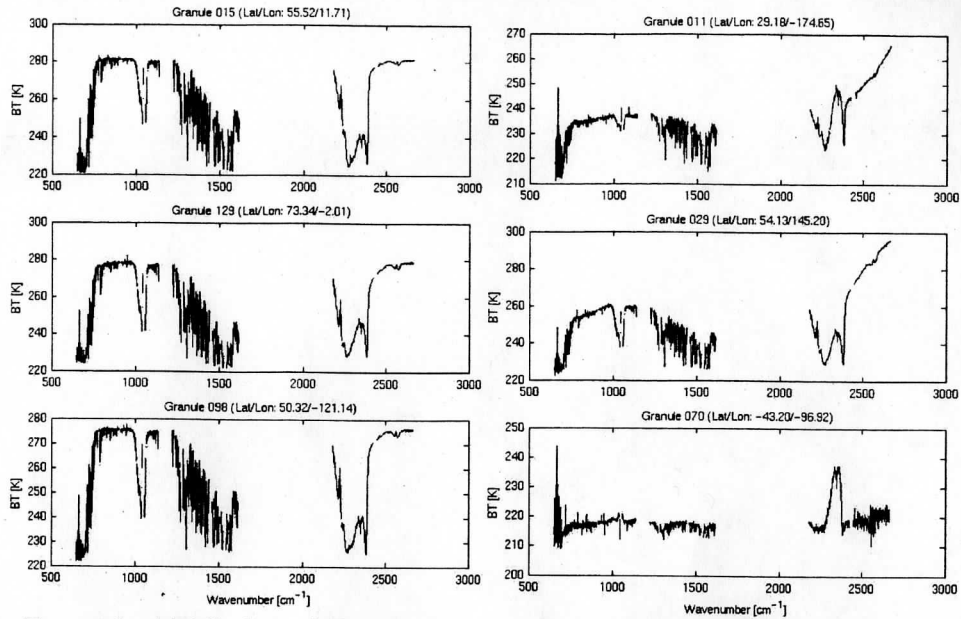
Fig. 2. Example AIRS clear (left column) and cloudy (right column) spectra showing the spectral differences due to cloud properties and their surrounding environments.

A global sampling of high spectral resolution AIRS spectra is shown in Fig. 3. Although the information content of infrared measurements appears to be perplexing, physical understanding, careful computer modeling, and appropriate assimilation strategies will provide the tools needed to assimilate these radiance data into NWP forecast models.
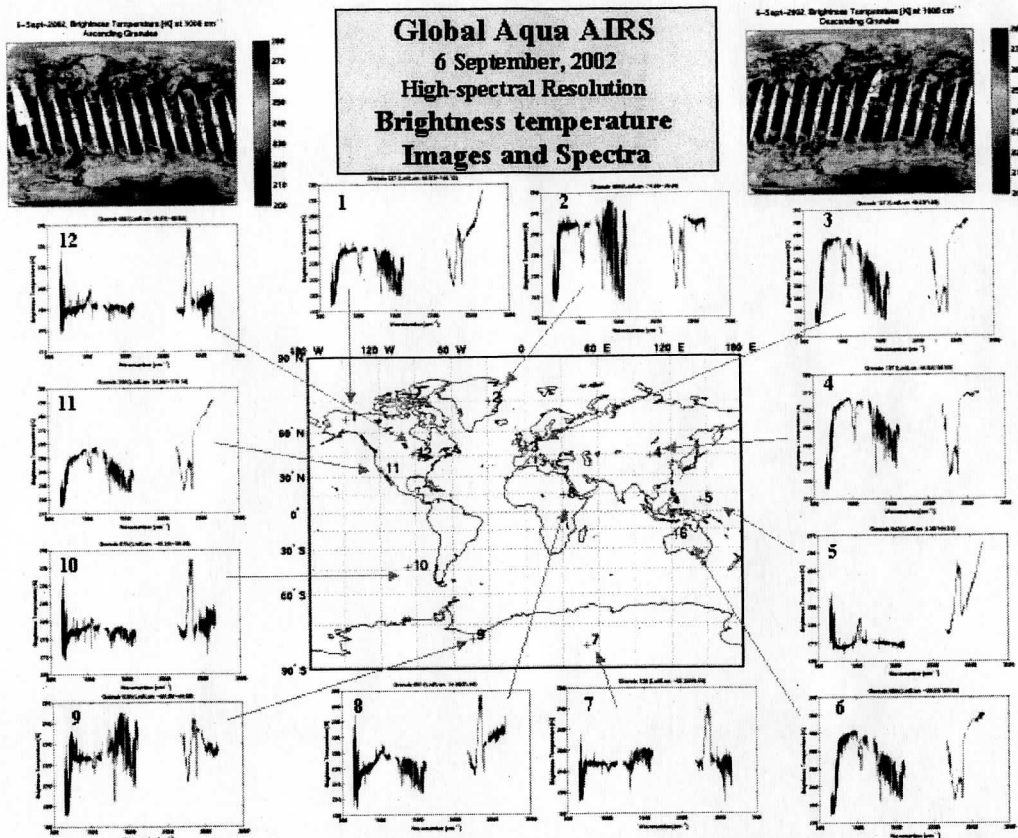
Fig. 3. Global AIRS spectra selected from 6 September 2002 to demonstrate the extraordinary wealth of measurements available to scientists for revealing subtle details of our earth-atmosphere system.

As an illustration, an observed cloudy spectrum (shown in black in fig. 4) is compared with different calculated spectra for various micro-physical properties, cloud particle sizes (effective diameters of 35, 45 and 60 microns) and cloud optical thicknesses (i.e., 1.20, 1.43 and 1.60). Assuming that the atmospheric conditions are known, one can calculate the cloudy scene spectra that match the measurements, within certain bounds of parameter uncertainty (Wei et al, 2004). This simple illustration demonstrates that our current understanding and theoretical modeling capability, which can be advanced to accurately retrieve the embedded cloud information, will enable future quantitative use of the cloudy scene radiance measurements for many applications, including NWP.
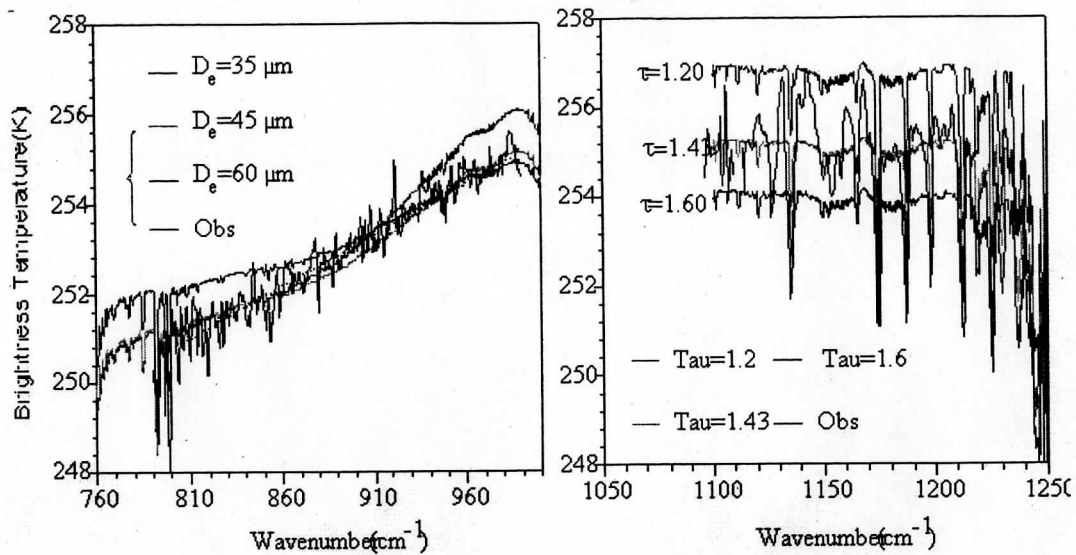
Fig. 4. Simultaneous retrieval of the effective size (D_e) and optical thickness (Tau) of ice clouds from HIS spectra. (Left) brightness temperature versus particle size assuming Tau=1.43, and (right) brightness temperature versus optical thickness assuming D_e is 45 microns (Huang et al., 2004)

3. Cloud Clearing Issues

Cloud clearing is an indirect approach to allow data assimilation or retrieval to use cloud contaminated measurements to represent clear sky atmospheric conditions either within or alongside partly cloudy areas. A single day of global ECMWF analyses and AIRS cloud cleared retrievals, provided by the AIRS science team, were used to demonstrate the information content. Figs. 5 and 6 are global coverage of the data used in the following analysis.
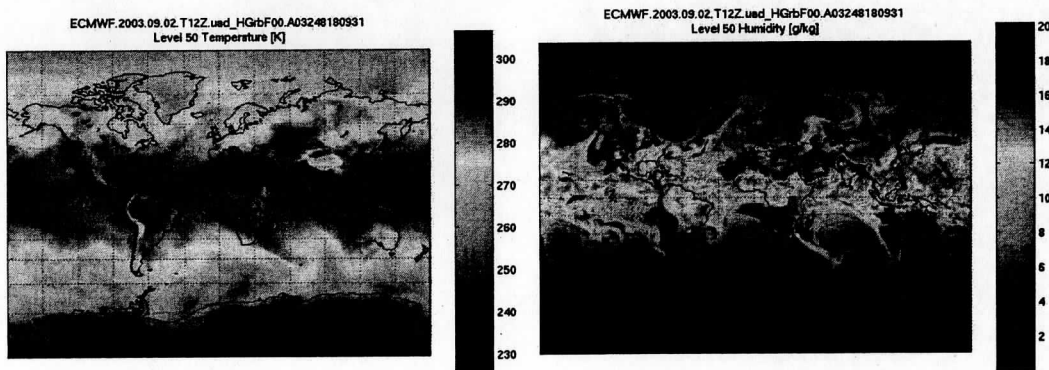
Fig. 5. ECMWF analyses of temperature (left) and water vapor (right) near the surface on 2 September 2003.
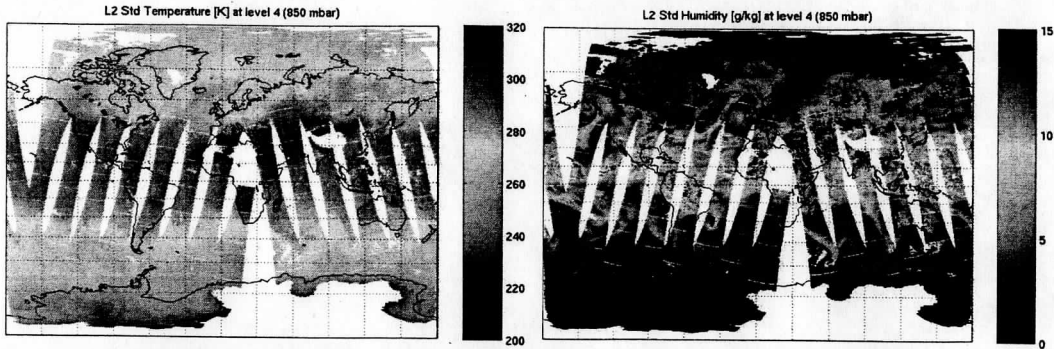
Fig. 6. AIRS cloud cleared radiance retrieved temperature (left) and water vapor (right) for the 850 mb level on 2 September 2003.

One day of ECMWF global analysis data (129960 profiles, half of the total available profiles) (fig. 7) and all available AIRS science team retrieval profiles taken during the same day (fig. 8) form a useful dataset for comparison. Comparing figures 7 and 8 shows that the global temperature structure is distinctly different under regions covered by clouds of differing phase. Unlike the analysis provided by ECMWF, the same day's AIRS cloud cleared radiance temperature retrieval structure has no distinction between clear and cloud cleared. This is precisely what cloud clearing is designed to achieve, that is, to produce retrievals of temperature profiles for the clear portion of the partly cloudy sky. However there is a consequence of representing the whole globe without clouds. Providing NWP models with only clear sky atmospheric profiles will severely bias the model fields since these conditions differ significantly from the ever-present partly cloudy sky condition.
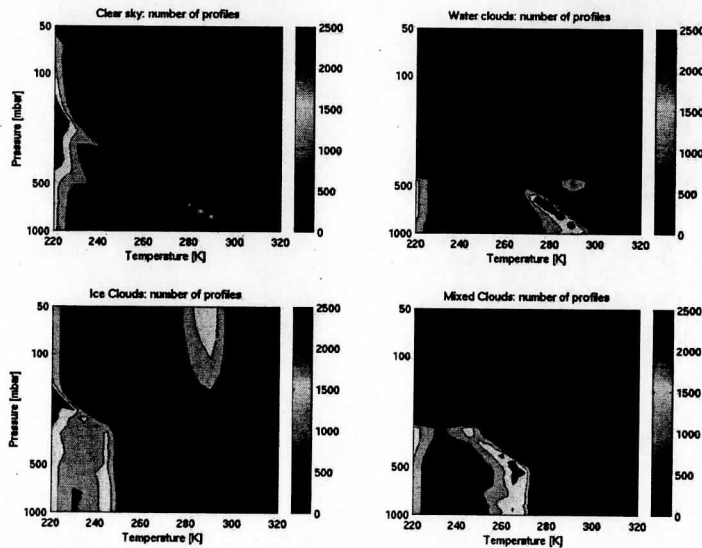
Fig. 7. Color contour histograms of ECMWF global temperature classified into (a) clear (upper left), (b) water cloud (upper right), (c) ice cloud (lower left) and (d) mixed phase (lower right) cloud according cloud information flag recorded in the analysis data file.
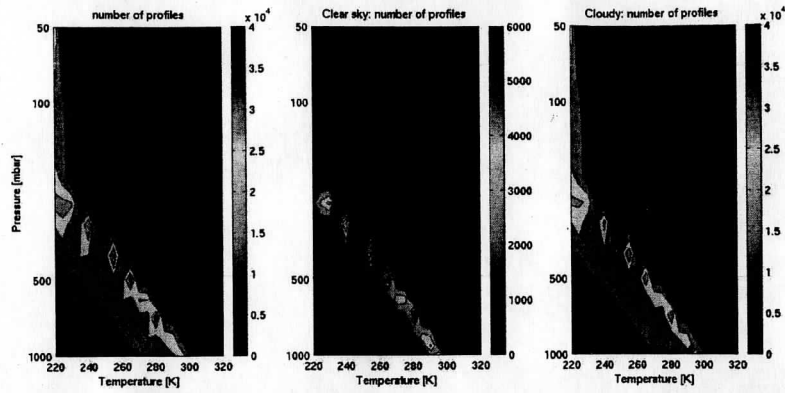
Fig. 8. Color contour histogram of AIRS science team standard temperature retrieval classified into (a) all (clear and cloud cleared combined, left panel), (b) clear (middle panel), and (c) cloud cleared (right panel) in the retrieval data file.

Figs. 9 and 10 show for water vapor features similar to that shown for temperature in figs. 7 and 8, respectively. The same conclusion can be reached, that is, AIRS clear and cloud cleared water vapor retrieval profiles are similar to the clear conditions shown in the ECMWF analysis. The clear water vapor profiles are vastly different from those associated with water, ice and mixed phase cloud conditions. NWP model assimilation of cloud cleared water vapor radiances will tend to produce a clear sky bias in the global humidity conditions.
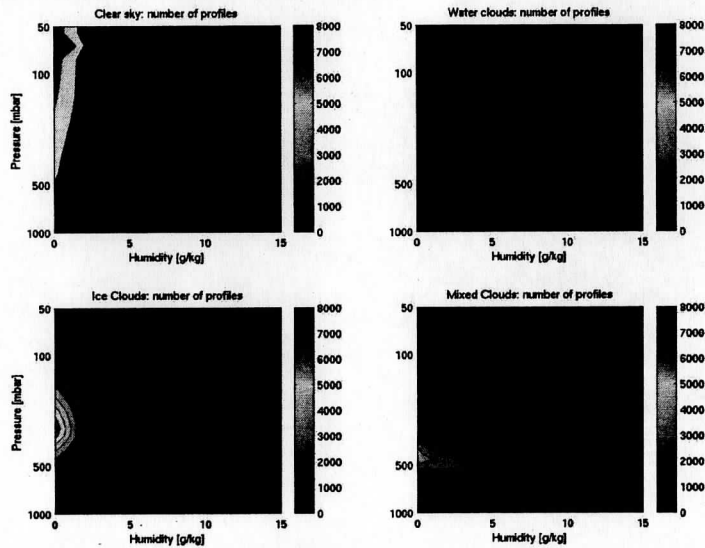
Fig. 9. As for fig. 7 except for water vapor profile.
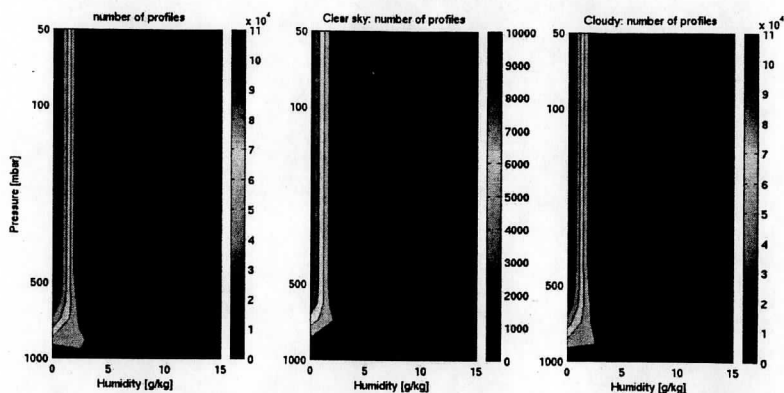
Fig. 10. As for fig. 8, except for water vapor profile.

Cloud-clearing Technique: Fig. 11 shows a grid of AIRS FOVs including a surrounding target area where a reference AIRS clear spectrum is identified using the MODIS cloud mask. A single AIRS FOV spectrum is defined as being clear if more than 95% of the MODIS pixels within the AIRS FOV are declared by the MODIS cloud mask as "confident clear". Such an AIRS spectrum is selected as "reference clear" and is used in evaluating the cloud cleared radiances derived from the 9 FOVs' "golf ball" within the interior of the grid shown in Fig. 11. If multiple "reference clear" AIRS FOVs are found, the warmest of these is selected as the final "reference clear".

To objectively validate the AIRS science team cloud cleared radiance performance, the following procedure is implemented:
Find at least one neighboring AIRS single FOV (S-FOV) within or surrounding the AIRS golf ball that is clear (according to MODIS cloud mask for which that within this FOV at least 99% is clear). In other words, from 25 candidates (fig. 11 below) find one clear AIRS FOV as the " clear ground truth" to estimate cloud clearing (CC) error.
Compute the bias (mean of differences), the Root Mean Square Error (RMSE), and Root Mean Square Difference (RMSD) spectra from all AIRS/AMSU golf ball CC radiances that have a corresponding clear S-FOV (as defined as above) radiance spectra.
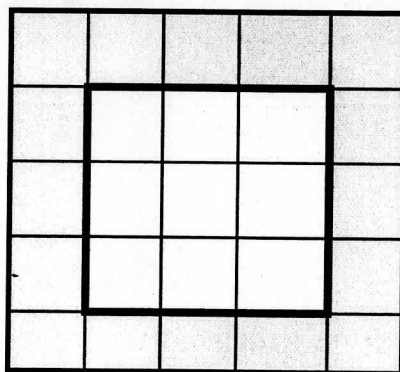
□ : AIRS golf Ball (3 by 3 S-FOV)

Fig. 11. AIRS golf ball (3 by 3 of AIRS single FOVs) and its surrounding FOVs used as a target area for finding the reference clear spectrum.

Fig. 12 shows 24 day and 24 night AIRS granules for 6 September 2002 on which day version 3.5.0 cloud cleared radiance granules were available for obtaining the error statistics.

Current* AIRS Cloudy Cloud Clearing Characteristic – Case Data Set

The selected granules of focus day of 6 September 2002 (so far cloud clearing <u>Ver. 3.5.0</u> data are available for AIRS focus days only) are used for the error estimate. <u>24 -day and 24 –night granules over ocean and land are:</u>

Day
G025, G027, G058, G060, G061, G075, G078, G092, G094, G108, G111, G126, G141, G144, G157, G159, G174, G192, G193, G207, G209, G224, G226, G239

Night
G115, G117, G100, G082, G083, G085 G065, G049, G052, G034, G036, G016 G017, G019, G001, G230, G214, G216 G197, G200, G182, G184, G148, G151

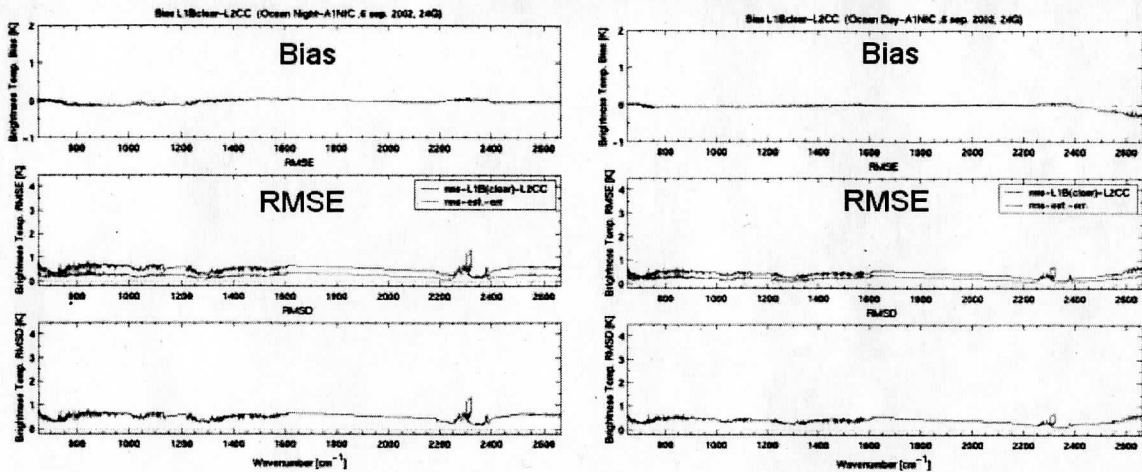*AIRS cloud clearing Version 3.5.0.0
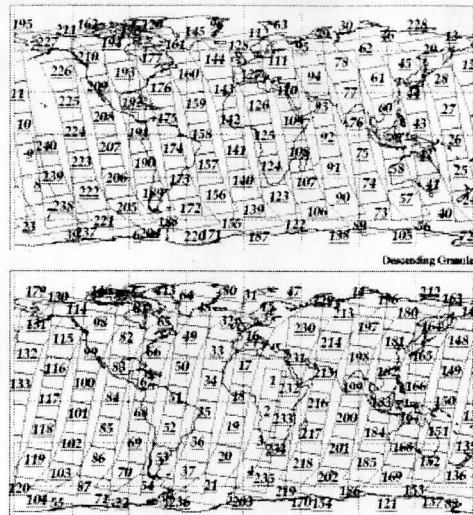
Fig. 12. Selected AIRS granules used in the calculation of cloud clearing radiance error.

Figs. 13 and 14 are the bias and RMSE of AIRS science team cloud cleared radiances derived from the selected granules shown in fig. 12 using the concept of "reference clear" as defined in fig. 11 and described above. Over ocean, shown in fig. 13, both day and night time, bias and RMSE of cloud cleared radiance errors are relatively small, although higher than the detector noise level, as required for high vertical resolution retrievals. In this case, the RMSE assessed here is a factor of two higher than the AIRS science team theoretical estimated levels (red curves). Thus, over ocean the AIRS/AMSU cloud clearing produces reasonable performance, but unfortunately the errors are still significantly larger than the noise level required to extract the highest vertical resolution information retrievable from the AIRS clear sky sounding radiances.

Current* AIRS Cloudy Cloud Clearing Characteristic – Case Study Result (Over Ocean)

Red curves are AIRS C.C. theoretical error estimate for comparison

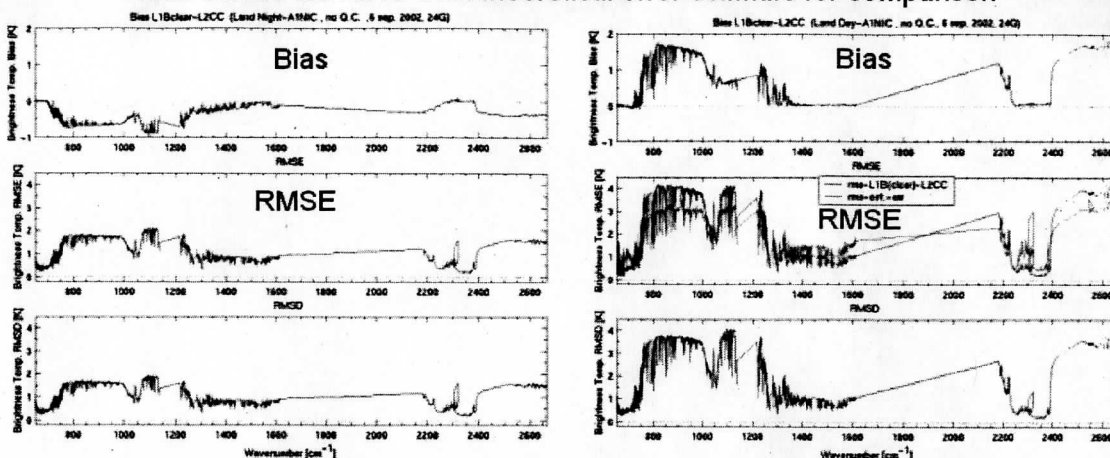**Nighttime – 1550/24 Sample Size/Granule   Daytime – 5071/24 Sample Size/Granule**

*AIRS cloud clearing Version 3.5.0.0

Fig. 13. Brightness temperature bias (upper panel) and RMSE (middle panel) of AIRS Version 3.5.0 cloud cleared radiances over ocean for nighttime (left) and daytime (right).

Over land areas the AIRS/AMSU science team cloud clearing error situation is much worse. Much higher errors, both in bias and RMSE, occur compared to the algorithm's over ocean counterpart. As a matter of fact, most of the cloud cleared radiances have very low yield (low number of cloud cleared retrievals pass its stringent quality control) and, as a result, all retrievals with or without passing quality control are used in the assessment of the cloud clearing error. The official AIRS science team's land estimated error (red curve in fig. 14) is also significantly higher than its ocean counterpart, consistent with the error estimated by the procedure used here. Looking further into the cloud clearing performance over land, one can find that the daytime results have significant degradation possibly due to the solar reflection of bright clouds and land surfaces and also due to the fact that there is a significant differential between surface skin and air temperatures which is not captured by the microwave data used as the clear sky information used for the cloud clearing procedure. In short, current AIRS/AMSU science team cloud clearing retrieval performs much better over ocean than over land areas, the poorest performance being for daytime viewing conditions. A major overhaul of the algorithm is now underway, but the case made here is that the use of AMSU data alone for the clear sky information used for AIRS cloud clearing is insufficient over land, particularly for daytime viewing conditions. On the other hand, co-located high spatial resolution MODIS infrared data may potentially complement AIRS/AMSU cloud clearing to achieve reliable performance over land and ocean regions alike.

Current* AIRS Cloudy Cloud Clearing Characteristic – Case Study Result (Over Land%)

Red curves are AIRS C.C. theoretical error estimate for comparison

Nighttime – 2612/24 Sample Size/Granule   **Daytime – 1745/24 Sample Size/Granule**

*AIRS cloud clearing Version 3.5.0.0   %With failed quality control data

Fig. 14. As for fig. 13 except errors are representing cloud cleared radiances over land only.

MODIS/AIRS synergistic (Smith et al., 2003) and AIRS/AMSU (Susskind et al, and Aumann et al, 2003) cloud cleared retrieval for one single granule over ocean and desert surface shown in fig. 15 are analyzed.

6 Sep 2002 focus day Granule 58 (Partial Land Day)
AIRS Cloud Mask (derived from co-located MODIS cloud mask)

West Coast of Australia

Brightness Temp.
*AIRS cloud clearing Version 3.5.0.0
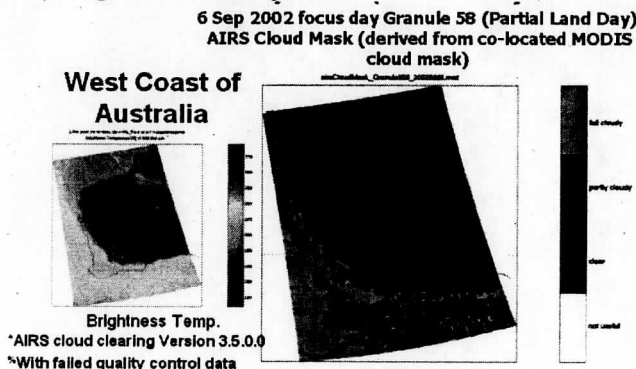%With failed quality control data

Fig. 15. AIRS window brightness granule (left) and AIRS single field of view cloud mask (right) image of 6 September 2002.

Bias and RMSE of cloud clearing error using AIRS/MODIS and AIRS/AMSU science team cloud cleared radiances are shown in fig. 16. For this case study AIRS/AMSU cloud clearing exhibits large bias and relatively large RMSE. Although AIRS/MODIS approach has slightly smaller RMSE than AIRS/AMSU it does have much smaller bias (near zero except for short wave region). The near zero bias of AIRS/MODIS cloud clearing approach is appealing for the NWP data assimilation application. The fact that there is a large cloud cleared (CC) radiance RMSE exhibited in the window regions of the spectra indicates that much of the magnitude of the CC radiance RMSE is due to surface skin temperature and emissivity spatial differences which exist between the

cloudy scenes (Huang et al, 2004) and the neighboring clear sky validation scenes. Such differences would be expected to exist over the Australian continent.
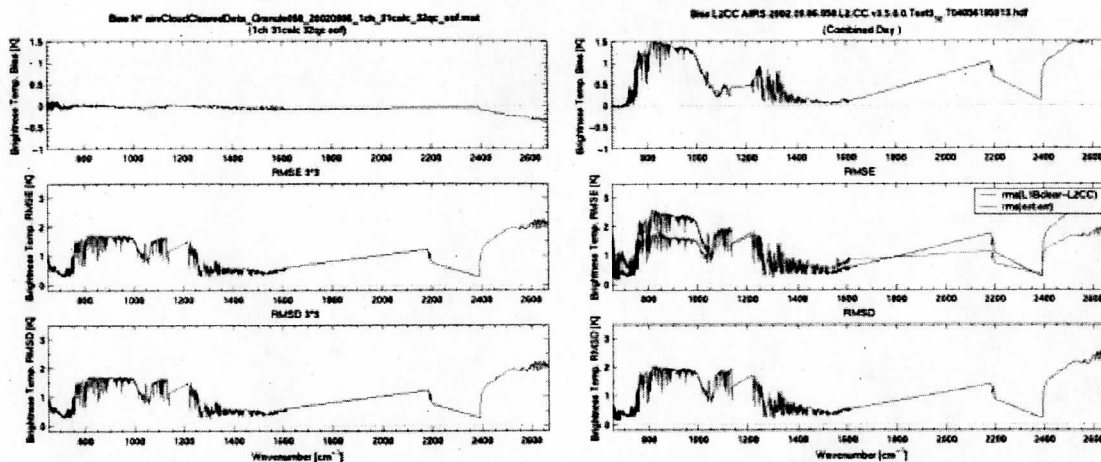

Fig 16. Comparisons of AIRS/MODIS (left panel) and AIRS/AMSU (right panel) cloud clearing error in terms of bias (upper panel) and RMSE (middle panel) derived from granule 58 of 6 September 2004. Note that red curve in the middle right middle panel is AIRS science team own estimated error.

In order to better illustrate the accuracy differences of the cloud cleared radiances derived from AIRS/AMSU and AIRS/MODIS, the cloud cleared AIRS radiances obtained from both approaches are convolved spectrally to simulate MODIS infrared band images of 20, 29, 31, and 33. The MODIS band spectral response functions used for the convolution are shown in Fig. 17.
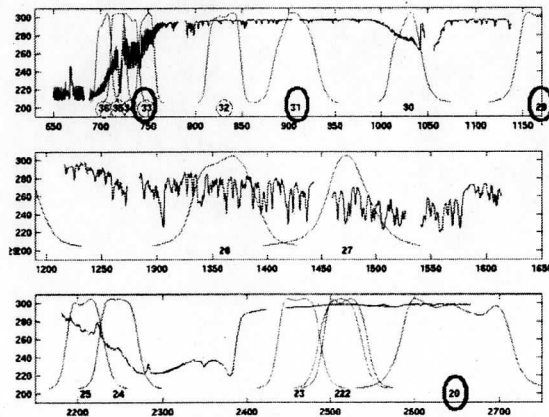

Fig. 17. MODIS spectral response functions with labeled band number used in the study.

In fig. 18, the MODIS band images simulated from the convolved AIRS cloud cleared radiances are compared with the actual MODIS clear single pixel images. The retrieved AIRS cloud cleared radiances convoluted with the MODIS spectral response functions should resemble the MODIS clear sky images observed during the same orbit time. Indeed the AIRS/MODIS cloud cleared brightness temperature image of all MODIS bands are shown to be very similar to that observed with MODIS. As can be seen, of the MODIS/AIRS cloud clearing approach captures all the small and large

spatial and spectral patterns that have been observed by MODIS. The lower resolution and highly unstable MODIS band images derived over land using the AIRS/AMSU cloud cleared radiances provide evidence that this is an unsatisfactory approach for deriving cloud cleared radiance over land areas of the globe.
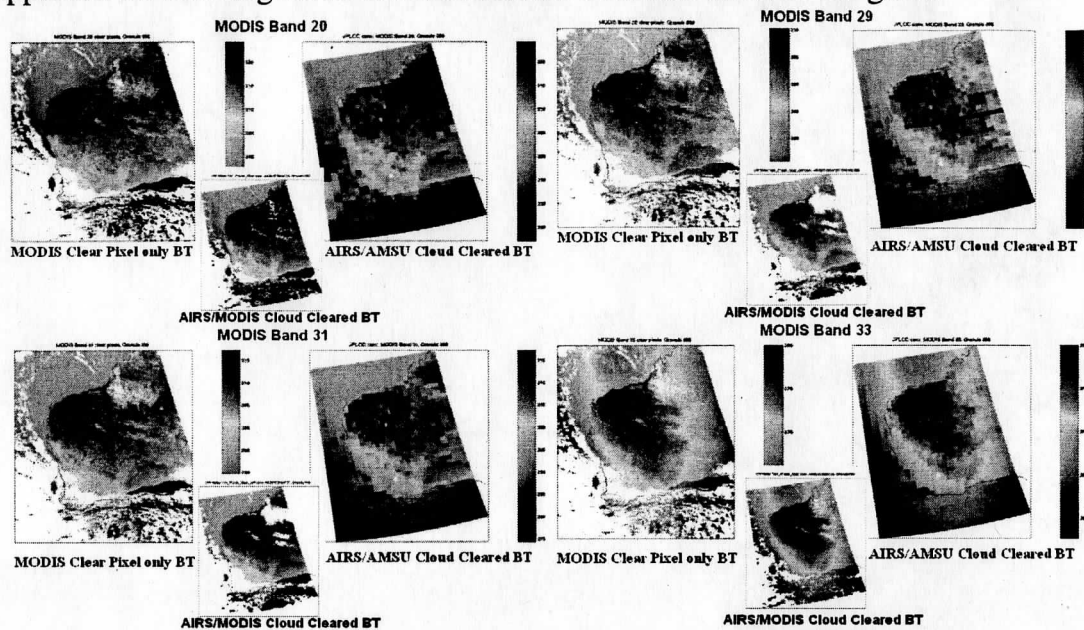

Fig. 18. Plots of brightness temperature of MODIS and AIRS/MODIS and AIRS/AMSU cloud cleared MODIS simulated images used to validate cloud clearing performance. Images of band 20 (upper left), band 29 (upper right), band 31 (lower left), and band 33 (lower right) are shown respectively. For each panel MODIS clear pixel (left), AIRS/MODIS cloud cleared MODIS simulated (middle), and AIRS/AMSU cloud cleared MODIS simulated (right) brightness temperature for the different MODIS bands are displayed.

4. Ultraspectral Infrared Cloud Forward Modeling

Building a comprehensive cloud property database that accounts for the single-scattering effects of ice and water clouds is essential for the modeling of cloudy infrared measurements (Huang et al 2003). The current database considers 7 shapes of ice crystals in the form of aggregates, solid hexagonal columns, droxtals, hollow columns, plates, bullet rosettes and spheroids. It also considers 38 size bins of particle ranging from 2 to 3100 microns in terms of particle maximum dimension. The database calculates 49 key wavelengths from 3.08 to 100 microns to cover all potential aircraft and space-borne multispectral, hyperspectral, and ultraspectral measurement specifications. The single scattering properties are used to parameterize cloud absorption and reflectance effects so that forward radiative transfer computations in the presence of cloud can proceed swiftly. The parameterized cloud albedo and transmissivity functions for ice clouds are derived as functions of optical thickness (ranging from 0.04 to 50), effective sizes (ranging from 10 to 157 microns), effective shape (from the list of the above 7 crystal habits), zenith angle (from 0 to 80 degrees), and of wavenumber (from 500 to 2500 1/cm). For water clouds, the optical thickness range is from 0.06 to 150 and the effective size from 2 to 20 microns.

These albedo and transmissivity databases are then used in the calculation of cloud component radiance to account for the scattering and absorption of clouds.

5. Summary and Conclusions

Based on the current infrared sounding instrument field of view (FOV) size >14 km, depending upon scan angle, the probability of cloud free single FOV measurements are less than 5 to 10 % at best. To improve the use of ultraspectral sounding data in numerical weather prediction model and generation of environmental and atmospheric products one must find ways to efficiently treat the effects of clouds. Unfortunately clouds greatly complicate the processing of ultraspectral infrared sounding data and, at present, a complete physical treatment of clouds is prohibitive. The computation of few thousands of cloudy radiances within each FOV is very time consuming when both absorption and scattering of clouds, and how these couple to clear air emission/absorption and earth surface reflection, need to be accounted for simultaneously.

Using AIRS cloudy data we have shown that spectral signatures of clouds are compounded by, not only the atmospheric variations (vertical inversion, horizontal temperature and water vapor gradient, solar reflection, etc), but also cloud in-homogeneity (multiple cloud layers and mixed phase sub-pixel elements), surface effects (spectral variation of surface emissivity and reflectivity) and local thermodynamic disequilibrium. Interpolation of clear and cloudy AIRS data becomes a complicated issue and the use of clear or cloud contaminated infrared data becomes the focal point of data preprocessing if this information source is to be assimilated or used to derive products in a timely fashion.

The cloud clearing approach generates spectral radiances as if they represented a clear portion of the measured partly cloudy area. The cloud clearing performance of the current AIRS science team algorithm using AIRS and AMSU is analyzed alone and with a synergistic AIRS and MODIS approach. Over ocean, the AIRS/AMSU cloud clearing performs in a reasonable manner in that the bias and root mean square error of cloud clear radiances compare favorably with nearby "cloud free" AIRS radiance spectra used here as the measure of the "clear truth". The AIRS science team theoretical estimated cloud clearing error is in reasonable agreement (i.e., within a factor of two) with this performance measure. However, current AIRS cloud clearing retrieval over land suffers from the surface effects (infrared emissivity and solar reflection). Case studies over land (especially over desert) are analyzed to demonstrate the advantages and drawbacks of both AIRS/AMSU and AIRS/MODIS synergistic approaches. This preliminary analysis has shown that the potential large bias and root mean square error of cloud clearing is indeed occurring over land areas using the AIRS/AMSU approach. The AIRS/MODIS approach, however, seems to be able to produce cloud cleared radiances much more reliably with smaller bias and random error. This was expected in that MODIS, unlike AMSU, sees the surface radiance in much the same manner that AIRS sees the surface (i.e., the proportion of clear scene and the surface emissivity characteristics are the same for MODIS and AIRS).

It is crucial to note that the above preliminary comparison and results are conducted using a large percentage of failed quality control AIRS/AMSU cloud cleared retrievals of Field of Regards (an FOR is an area covered by a 3 by 3 array of single FOVs, also referred to as "golf balls") for evaluation of both AIRS/AMSU and AIRS/MODIS (at 1 by 2 FOV resolution) cloud clearing retrieval performance. Although a fair comparison, one must keep in mind that it is not using the latest AIRS/AMSU science team cloud clearing retrieval that has still not been validated and is currently undergoing major algorithm overhaul.

While major efforts and advances have been made in the AIRS/AMSU and, more recently, the AIRS/MODIS cloud clearing retrieval, cloud clearing by definition accounts for the cloud effects with a clear sky replacement strategy. Cloud cleared radiances and their associated sounding profiles, in practice, cannot represent cloudy sky sounding nor should be directly assimilated into a numerical weather model without the necessary ancillary cloud information. The example single day of ECMWF analysis and AIRS/AMSU cloud cleared retrieval profiles have demonstrated the argument that AIRS/AMSU cloud cleared sounding profile, both temperature and water vapor, are distinctly different from the cloudy profiles exhibited by the ECMWF analysis. Replacing the whole globe of cloudy profiles with cloud cleared profiles, without the benefit of ancillary cloud property data, is essentially providing the NWP model with initial states not consistent with the truth.

The needs for improving the yield of AIRS data used in numerical weather prediction models and for producing global sounding retrieval are urgent. Complicated and novel approaches to the assimilation of cloudy infrared radiances should be examined. At present University of Wisconsin-Madison is partnering with Texas A&M University to develop a physically based fast parameterized cloudy infrared ultraspectral forward model that is both fast and sufficiently accurate to allow future direct assimilation and retrieval of cloudy data without other preprocessing such as cloud clearing. Preliminary cloud microphysical parameterization approach (Yang et al., 2001 and 2004) can be summarized as:

- Cloud single scattering properties are computed by rigorous composite models, such as the finite-difference time-domain (FDTD) technique, the T-matrix method and an improved geometric optics method (IGOM) for nonspherical ice crystals, and the Lorenz-Mie solution for "equivalent" ice spheres.
- Seven ice crystal habits (aggregate, hexagonal column, hexagonal plate, bullet rosette, hexagonal hollow column, spheroid, and droxtal) are considered.
- A database of the single-scattering properties of ice crystals at the infrared spectrum, from 3 to 100 μm, and a particle size spectrum from 2 μm to 10000 μm in terms of the particle maximum dimension are generated.
- Parameterized cloud transmissivity and reflectivity are derived to account for the multiple scattering effects due to clouds.
- Fast infrared gaseous absorption forward model is modified to include cloud transmissivity and reflectivity to form fast parameterized cloudy model.

- "True" cloudy forward model calculations are performed by LBLRTM follow by the DISORT multiple scattering to accurately account for both gases and clouds effects in deriving the top of atmosphere radiances to characterize the accuracy of the fast parameterized cloudy forward model.
- Fast cloudy forward model performance is estimated by the comparison of the differences between the cloud radiances of this fast model and the "true" model.
- Improved cloud parameterization will be necessary if testing against the "true" model shows difference above NWP threshold requirements.

An application of these cloud radiative transfer models to AIRS retrievals has already been conducted by Smith et al 2004.

In summary, in order to assimilate cloudy radiances into numerical weather prediction models, besides using clear channels selected within each FOV, two candidate approaches are: (1) an indirect method whereby clear sky equivalent radiances are derived, and (2) a direct method in which the actual cloud radiances are assimilated. For the indirect method of assimilating cloud cleared radiances, great care must be taken, since it has been demonstrated that the direct assimilation of clear radiances that are located in the cloudy regions have the potential for clear sky bias which will negatively impact NWP analyses and forecasts. In these assimilation regions, the associated cloud parameters, such as cloud height and optical properties, and associated cloudy sky thermodynamic characteristics, must accompany cloud-cleared radiances. The new and challenging task becomes the inclusion of cloud properties and associated atmospheric thermodynamic characteristics using assimilation in the current model.

In the direct cloudy radiance assimilation method, a parameterized cloudy forward model that is both fast and accurate is needed. Thus far, only limited work has been carried out and a significant research and development effort is still needed in order to implement a method for the direct assimilation of cloud contaminated radiance observations. The limitation of the accuracy of the fast cloudy sky radiative transfer model and its practical application into the radiance assimilation process require considerable study and attention.

References

Aumann, Hartmut H.; Chahine, Moustafa T.; Gautier, Catherine; Goldberg, Mitchell D.; Kalnay, Eugenia; McMillin, Larry M.; Revercomb, Hank; Rosenkranz, Philip W.; Smith, William L.; Staelin, David H.; Strow, L. Larrabee, and Susskind, Joel. AIRS/AMSU/HSB on the Aqua Mission: Design, science objectives, data products, and processing systems. IEEE Transactions on Geoscience and Remote Sensing v.41, no.2, 2003, pp253-264.

Huang, Hung-Lung; Tobin, Dave; Li, Jun; Olson, Erik; Baggett, Kevin; Huang, Bormin; Mecikalski, John; Knuteson, Bob; Osborne, Brian; Posselt, Derek; Antonelli, Paolo; Revercomb, Hank; Smith, William, and Yang, Ping. "Hyperspectral radiance simulator - cloud radiance modeling and beyond". Optical Remote Sensing of the Atmosphere and Clouds III, Hangzhou, China, 25-27 October 2002. Bellingham, WA, International Society for Optical Engineering, (SPIE), 2003, pp180-189. Reprint #3477.

Huang, H-L, W.L. Smith, J. Li, P. Antonelli, X. Wu, R.O. Knuteson, B. Huang, B.J. Osborne, 2004: Minimum Local Emissivity Variance Retrieval of Cloud Altitude and Emissivity Spectrum – Simulation and Initial Verification. *J. Appl. Meteor._*May, 795-809.

Huang, H-L, P. Yang, H.-L. Wei, B. A. Baum, Y.-X. Hu, P. Antonelli, and S. A. Ackerman, "Retrieval of ice cloud properties from high spectral resolution infrared observations," *IEEE Trans. Geosci. Remote Sensing*, vol. 42, pp. 842-853, 2004.

Smith, W. L., G. E. Bingham, G. W. Cantwell, M. J. Gordon, D. K. Zhou, and H-L. Huang, 2003: "AIRS Cloud-clearing Using Multi-spectral MODIS Imagery", Available from bill.l.smith@cox.net

Smith, W. L., and D. K. Zhou, H-L Huang, Jun Li, X. Liu, and A. M. Larar, 2004: "Extraction of Profile Information from Cloud Contaminated Radiances", Proceedings of the ECMWF Workshop on the Assimilation of High Spectral Resolution Sounders in NWP, June 28 – July 1, 2004.

Susskind, J., C.D. Barnet, and J.M. Blaisdell, 2003: Retrieval of Atmospheric and Surface Parameters from AIRS/AMSU/HSB Data in the Presence of Clouds. IEEE Transactions pf Geoscience and Remore Sensing, Vol. 41, No. 2, February, 390-409.

Wei H., P. Yang, J. Li, B. A. Baum, H.-L. Huang, S. Platnick, Y. X. Hu, and L. Strow, "Retrieval of semi-transparent ice cloud optical thickness from Atmospheric Infrared Sounder (AIRS) measurements," *IEEE Trans Geosci. and Remote Sensing*, 2004 (in press).

Yang P., B. C. Gao, B. A. Baum, Y. Hu, W. Wiscombe, S.-C. Tsay, D. M. Winker, S. L. Nasiri, 2001: Radiative Properties of cirrus clouds in the infrared (8-13 um) spectral region, *J. Quant. Spectros. Radiat. Transfer*, 70, 473-504.

Yang P., H. Wei, H.-L. Huang, B. A. Baum, Yong X. Hu, K. N. Liou, M. I. Mishchenko, and Qiang Fu, 2004: Database and parameterization of the single-scattering properties of ice crystals at infrared wavelengths. Manuscript prepared for submission to Applied Optics.

Inference of ice cloud properties from high-spectral resolution infrared observations

Hung-Lung Huang[1], Ping Yang[2], Heli Wei[2], Bryan A. Baum[3,1], Yongxiang Hu[3],

Paolo Antonelli[1], Steven A. Ackerman[1]

[1] Cooperative Institute for Meteorological Satellite Studies, University of Wisconsin-

Madison, 1225 W. Dayton Street, Madison, WI 53706

[2] Texas A&M University, Department of Atmospheric Sciences, TX 77843

[3] NASA Langley Research Center, Hampton, VA 23681

Corresponding author address: Dr. Ping Yang, Department of Atmospheric Sciences,

Texas A&M University, TAMU 3150, College Station, TX 77843-3150. Tel: 979-845-

4923; Fax: 979-862-4466; Email: pyang@ariel.met.tamu.edu

Abstract

The theoretical basis is explored for inferring the microphysical properties of ice crystal from high-spectral resolution infrared observations. A radiative transfer model is employed to simulate spectral radiances to address relevant issues. The extinction and absorption efficiencies of individual ice crystals, assumed as hexagonal columns for large particles and droxtals for small particles, are computed from a combination of the finite-difference time-domain (FDTD) technique and a composite method. The corresponding phase functions are computed from a combination of FDTD and an improved geometric optics method (IGOM). Bulk scattering properties are derived by averaging the single-scattering properties of individual particles for 30 particle size distributions developed from *in situ* measurements and for additional four analytical Gamma size distributions for small particles. The nonsphericity of ice crystals is shown to have a significant impact on the radiative signatures in the infrared (IR) spectrum; the spherical particle approximation for inferring ice cloud properties may result in an overestimation of the optical thickness and an inaccurate retrieval of effective particle size. Furthermore, we show that the error associated with the use of the Henyey-Greenstein phase function can be as larger as 1 K in terms of brightness temperature for larger particle effective size at some strong scattering wavenumbers. For small particles, the difference between the two phase functions is much less, with brightness temperatures generally differing by less than 0.4 K.

The simulations undertaken in this study show that the slope of the IR brightness temperature spectrum between 790–960 cm^{-1} is sensitive to the effective particle size. Furthermore, a strong sensitivity of IR brightness temperature to cloud optical thickness is noted within the 1050–1250 cm^{-1} region. Based on this spectral feature, a technique is presented for the simultaneous retrieval of the visible optical thickness and effective particle size from high spectral resolution infrared data under ice cloudy condition. The error analysis shows that the uncertainty of the retrieved optical thickness and effective particle size has a small range of variation. The error for retrieving particle size in conjunction with an uncertainty of 5 K in cloud temperature, or a surface temperature uncertainty of 2.5 K, is less than 15%. The corresponding error in the uncertainty of optical thickness is within 5-20%, depending on the value of cloud optical thickness. The applicability of the technique is demonstrated using the aircraft–based High-resolution Interferometer Sounder (HIS) data from the Subsonic Aircraft: Contrail and Cloud Effects Special Study (SUCCESS) in 1996 and the First ISCCP Regional Experiment - Arctic Clouds Experiment (FIRE-ACE) in 1998.

1. Introduction

Cirrus clouds play an important role in our climate system [1-4] yet their full impact on weather and climate change remains a puzzle. Substantial efforts have focused on remote sensing of cirrus clouds. Radiances observed by satellite-borne sensors at visible, near-infrared and mid-infrared wavelengths are widely used to retrieve cloud properties [5-9]. Emitted infrared radiation (IR), particularly in the atmospheric window region (i.e. 8-12 μm), contains a wealth of information on the properties of ice clouds. In the near future our ability to observe these global clouds will improve with the launch of new satellite instruments, such as the Geosynchronous Imaging Fourier Transform Spectrometer

(GIFTS) [10-11] and Cross-Track Infrared Sounder (CrIS) [12], that have high spectral resolution.

The high spectral resolution radiance spectrum contains some important information of cirrus clouds. The radiance at high spectral resolution over abroad wavelength range will lead improved cirrus clouds retrievals. High-resolution spectral signatures in the atmospheric window region have been used previously to study cloud and aerosol properties. Ou et al. [13] presented an algorithm to infer cirrus cloud properties from Airborne Remote Earth Sensing system (ARES) data within two mid-IR atmospheric window (5.1-5.3 μm and 3.7 μm) bands. Various IR algorithms to infer ice cloud properties based on radiances within the 8-12 μm atmospheric window have been suggested (see references [14-16]). A number of these studies, such as *Chung et al.* [14] and *DeSlover et al.* [17], approximated ice particles as spheres for the determination of scattering properties. However, *Kahn et al.* [18] found that radiative transfer simulations performed with nonspherical ice particle scattering models fit observed transmission spectra more accurately than simulations based on the spherical approximation employed in light scattering computation. A similar conclusion was reached by *Eldering et al.* [19] who used high-resolution spectra of non-gas-absorption transmission from Atmospheric Trace Molecule Spectroscopy Experiment (ATMOS) sun occultation data for cirrus cloud identification. *Rathke and Fischer* [20] presented an algorithm for inferring water cloud microphysical properties from high-resolution IR spectra, and investigated the sensitivity of the retrievals for clouds of moderate optical thickness.

The intent of the present study is to explore an approach for simultaneously retrieving cirrus cloud microphysical properties from the aircraft-based interferometer measurements in the 750–1250 cm^{-1} (i.e. 8-13.3 μm) spectral region. The present algorithm developed for retrieving cloud properties is complementary to the approaches based on the visible and near-IR spectral signatures reported by Nakajima and King [5], King et al. [6] and Platnick et al. [7].

This paper proceeds as follows. Section 2 presents the methodology for deriving the single-scattering properties of ice crystals and the numerical model for IR radiative transfer. This section also discusses the effect of ice crystal non-sphericity and the Henyey-Greenstein (H-G) phase function assumption on the radiative properties of ice crystals in the IR atmospheric window region. Section 3 presents the theoretical basis for inferring the microphysical and optical properties of ice clouds. Various sensitivity studies are carried out to understand the sensitivity of simulated brightness temperatures to the optical thickness and particle effective size of ice clouds. An error analysis for our algorithm is also presented in Section 3 where various factors that affect the retrieval accuracy are discussed. Shown in Section 4 are two example cases for the simultaneous retrieval of the ice cloud effective particle size and optical thickness that were observed during the SUCCESS in 1996 and the FIRE-ACE in 1998. Finally, the study is summarized in Section 6.

2. Single Scattering Properties of Ice Clouds and Radiative Transfer Simulations

To infer cloud properties from satellite- or aircraft-borne measurements using IR interferometer data, the radiance measurements are compared to theoretical simulations using a radiative transfer model (including a single-scattering module) that we describe in this section.

2.1 Single-scattering Properties of Ice /Cirrus Clouds

Scattering by ice crystals in the IR spectral region is non-negligible [21]. Although various *in- situ* observations have demonstrated that ice clouds are almost exclusively composed of nonspherical ice crystals (e.g. [22-23]), studies involving IR radiance measurements often assume ice particles to be spherical. Simulation studies by *Chung et al.* [14] found that the assumption of a spherical geometry for ice crystals may be adequate for very small ice crystals at IR wavelengths.

Heymsfield and Iaquinta [23] showed that in the upper portions of cirrus clouds, where the temperatures tend to be cold, the ice particles are small. Although these small particles are nonspherical, they tend to have aspect ratios (the ratio of particle length to its width) close to unity. *Yang et al.* [24] suggested the shape of small ice crystals may be represented by the droxtal geometry. *In-situ* measurements from the First ISCCP (International Satellite Cloud Climatology Project) Regional Experiment-II (FIRE-II) held in Coffeyville, Kansas in 1991, have shown that the middle to upper layers of midlatitude cirrus clouds are often composed of droxtals and pristine hexagonal crystals (see Fig. 15 of reference [23]). This is an important observation since the upwelling radiance in the IR spectral region tends to be dominated by absorption and scattering from the middle to upper regions of the cloud.

In this study, we use droxtals to represent small particles with size up to 32 μm in terms of maximum dimension, and hexagonal columns to represent larger particles. A number of investigators assume that ice crystals are hexagonal, which is a traditional non-spherical particle. Yang et al. [25] explained the use of hexagonal ice crystals for radiative transport through cirrus clouds.

Scattering and absorption properties of droxtals and small hexagonal ice crystals are calculated using the finite-difference time-domain (FDTD) method [26]. Figure 1 shows a comparison of the scattering phase functions at 1250 cm^{-1} for spherical, droxtal and hexagonal (with an aspect ratio of 1) ice crystal particles with the same maximum dimension of 10 μm. The phase function of the spherical particle was calculated from Lorenz-Mie theory using the computation code developed by *Wiscombe* [27]. As shown in Fig. 1, the scattering phase function is different for the three particle geometries in forward and backward directions. The forward scattering by droxtals is smaller than that by either hexagonal or spherical crystals because the volume of the droxtal is the smallest for the same maximum dimension. The positions of scattering sub-maximum are different
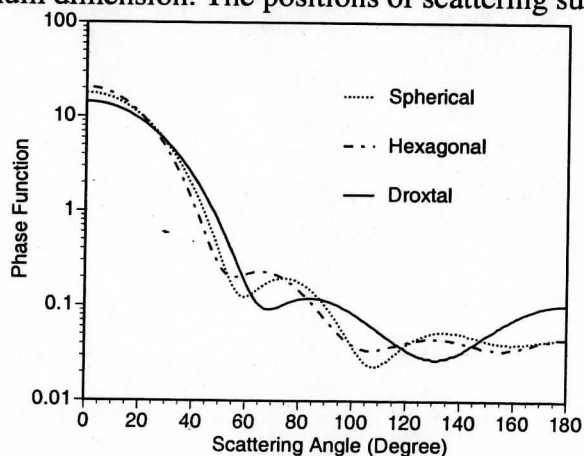
for different shapes.

Figure 1. Comparison of phase functions for droxtals, hexagonal columns, and spherical ice crystals with maximum dimension 10 μm at a wavenumber of 1250 cm^{-1} (wavelength 8.0 μm).

The extinction and absorption efficiencies for crystals ranging from 35 to 10,000 µm in size are derived on the basis of the composite approach reported in Fu et al. [28]. This approach uses FDTD or other accurate method to calculate the single-scattering properties for small particles, and the weighted summation of approximate methods (such as geometric optics method (GOM) and equivalent Mie theory) to calculate the single-scattering properties for moderate to large particles. The corresponding phase functions for larger particle sizes are derived from an improved geometric optics (IGOM) [29]. We noticed that the difference between the phase function computed from IGOM and that from an asymptotic solution [30] are quit similar for the spectral region involved in this study, if the size of the crystal are larger than approximately 40 µm. A recent study by Lee et al. [31] has confirmed the applicability of the IGOM for IR phase function computations in the case of circular cylinders, as validated by the T-matrix [32] method in the case of circular cylinders.

The bulk ice cloud single-scattering properties are obtained by integrating the individual crystal scattering properties over 30 particle size distributions obtained during various campaigns for various ice clouds systems from Fu [33] and Mitchell et al[34]. Because no *in-situ* measurements are available for clouds at extremely low temperatures (expected to contain primarily small ice particles), we assume very cold clouds composed of small particles to follow Gamma analytical distributions with effective sizes of 6, 8, 10 and 12 µm. Fu and Sun [35] find that the retrieval of D_e is also sensitive to the ice particle size distribution assumed for ice crystal. The cirrus clouds at different geographic regions may have different size distributions due to differences in the thermodynamic and dynamic environments in which they form. This requires that a broad set of cirrus particle size distributions are needed in the retrieval process. The impact of the particle size distribution on the retrieval result deserves further study

The ice cloud bulk single-scattering properties are parameterized based on the effective particle size of the 34 size distributions. The effective size is defined as the 1.5 times of the ratio of average volume of ice crystal particles to their average projected area. Figure 2 shows the mean single-scattering properties (extinction efficiency, absorption efficiency, and asymmetry factor) for four effective sizes of ice clouds (D_e=10, 30, 50 and 80 µm) within the spectral range 750–1250 cm^{-1}. The calculations shown in Fig. 2 were performed using the parameterization scheme developed by *Yang et al.* [25] for the optical properties of ice crystals.
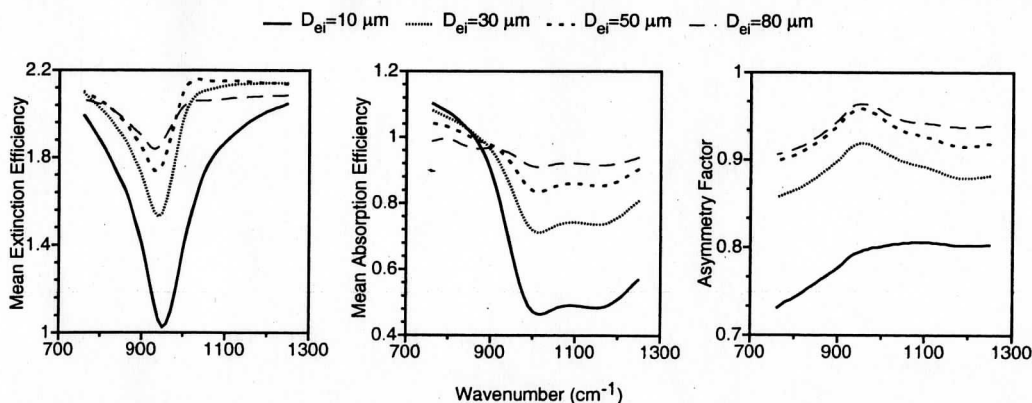

Figure 2. Single-scattering properties of ice clouds for four effective particle sizes

The mean extinction efficiency of ice crystals depends strongly on wavenumber, particularly, for small particle sizes. The extinction minimum at 950 cm^{-1}, which becomes more pronounced with decreasing particle size, corresponds to the Christiansen band of ice [36-37]. For large particle sizes (D_e=50 or 80 μm), the spectral variation of the extinction efficiency is relatively smooth. The total extinction efficiency of ice crystals (i.e., the sum of scattering and absorption effects) in the 1000–1250 cm^{-1} spectral region is nearly independent of effective particle size for large particles, a characteristic that is useful for the retrieval of ice cloud optical thickness.

The bulk absorption efficiency is related to the imaginary component of the refractive index of ice. In addition, the absorption of ice crystals depends on wavenumber and the effective particle size of the particles. The absorption efficiency varies with wavenumber in the 750–1000 cm^{-1} spectral region, particularly for small ice particles. This feature is useful for determining the effective size of ice crystals from high-resolution IR atmospheric spectral measurements. The asymmetry factor increases with effective particle size in the IR spectral region, implying that the scattering of the incident radiation by ice crystals is typically in the forward direction.

For water clouds, the bulk single scattering properties were calculated using the Lorenz-Mie theory [26], and assuming Gamma particle size distributions. The scattering properties of spherical particles have been extensively discussed by Hansen and Travis [38].

2.2 Numerical simulation of upwelling infrared radiances at aircraft level

Clear-sky (non-cloudy) monochromatic atmospheric molecular absorption optical thicknesses are computed from a line-by-line (LBL) radiative transfer model originally developed by Chou and Kouvaris [39]. For the present application, the atmosphere is divided into one hundred layers between the surface and an altitude of 20 km. Rawinsonde profiles provide atmospheric temperature, pressure, density and water vapor; the spectral line parameters of atmospheric gases are from HITRAN 2000 [40]; and the Voigt line shape [41] that accounts for both pressure and temperature broadening effects is used for computing the line absorption of atmospheric gas molecules. The continuum absorption of water vapor and other gases within 750–1250 cm^{-1} are calculated using the CKD-2.4 model [42]. To facilitate later comparisons with HIS data needed in the implementation of the retrieval technique, the monochromatic total optical thicknesses of atmospheric gases at every level are convolved with the instrumental response function. The upwelling atmospheric radiative spectrum under cloudy conditions at the aircraft altitude (20 km) is then computed in terms of brightness temperature by combining the clear-sky optical thickness from the LBL code and the discrete ordinates method radiative transfer (DISORT) [43]. Clouds are simulated by adding an optical thickness, single-scattering albedo, and scattering phase function into a model layer atmosphere. The DISORT method is used with 16 streams in calculations. The spectral interval is 0.2cm^{-1}. The Legendre extension coefficients of the phase function of ice crystals are derived using Hu's algorithm that properly accounts for the truncation of the strong forward peak [44].

2.3 Effect of Ice Crystal Nonsphericity

The significance of ice crystal nonsphericity in the retrieval of cloud optical thickness at visible and near infrared wavelengths has been discussed by Mishchenko et al. [45,46], Takano et al. [47] and references cited therein. Here we investigate the effect of ice

crystal nonsphericity on high-resolution IR spectral radiance simulations. Based on the single-scattering properties for same size distributions of both ice spheres and the hexagonal ice crystals, two sets of spectral-dependent brightness temperatures are calculated as functions of wavenumber. The visible optical thickness is fixed at 1 for these simulations. The two sets of resulting brightness temperatures for each size distribution are then differenced, with the results shown in Fig. 3 for the 800–1000 cm^{-1} spectral region. The brightness temperatures for spherical ice particles are 0.5–2.6 K lower than that for non-spherical particles. This is caused by the overestimation of the absorption and extinction efficiencies that occurs with the use of the spherical approximation [37].
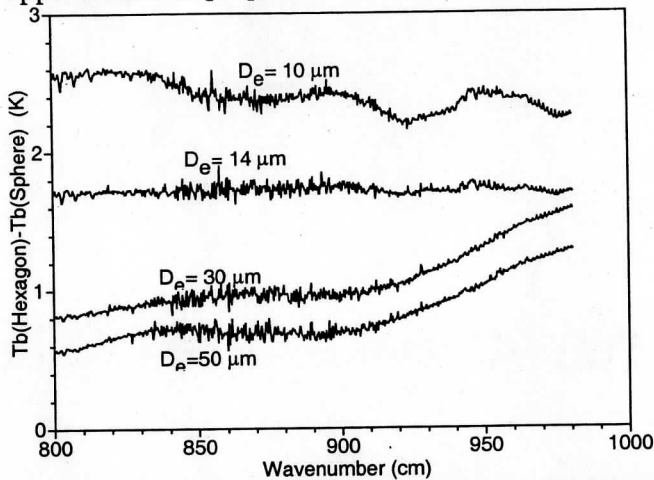
Figure 3. Shown are the differences in simulated upwelling brightness temperatures calculated for hexagonal ice crystals and spherical particles as a function of wavenumber for four effective sizes of ice clouds, but for a fixed cloud optical thickness of 1. Two sets of spectral brightness temperatures are calculated as a function of wavenumber based on the single-scattering properties for four particle size distributions of both ice spheres and the hexagonal ice crystals. The two sets of resulting brightness temperature spectra for each size distribution are then differenced. The atmospheric profiles are provided from a nearby rawinsonde. The surface skin temperature is 267.6 K and the cloud altitude is 7 km.

The previous results were obtained for a fixed optical thickness, but similar calculations can be made in which the particle size is fixed but the optical thickness varies. The results in Fig. 4 show the difference in spectral brightness temperatures calculated for three values of optical thickness within the 1100–1250 cm^{-1} spectral region, but for these simulations the effective particle size is fixed at 14 μm. The brightness temperatures for spherical ice particles are 1–2 K lower than that for non-spherical particles, depending on the optical thickness of the cloud.
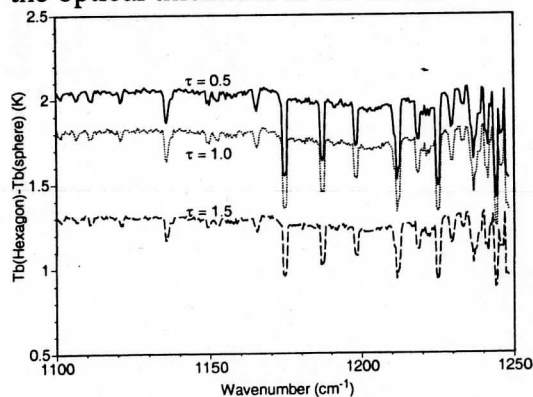
Figure 4. Shown are the differences in simulated upwelling brightness temperature spectra computed for hexagonal ice crystals and spherical particles. The brightness temperature differences are presented as a function of wavenumber for three cloud optical thicknesses. The effective particle size is fixed at 14 μm.

Figures 3 and 4 demonstrate that the nonsphericity of ice crystals can have a significant effect on the IR optical properties and that the spherical particle approximation for inferring ice cloud properties may result in an overestimation of the optical thickness and an inaccurate retrieval of effective particle size.

2.4 Errors caused by the use of the Henyey-Greenstein Phase Function

The impact of the nonspherical ice particles on optical properties raises the question of using a simplified form of the phase function in the radiative transfer simulations. Due to its simplicity and efficiency, the H-G phase function is widely used in the IR radiative transfer calculations as an approximation for describing the phase function of cloud particles. In this section we compare the H-G phase function with more realistic phase function calculated for hexagonal ice crystals from the FDTD and an improved geometric optics methods. The phase functions for individual crystals are averaged over the 34 ice cloud size distributions as discussed previously. For two different size distributions, Fig.5 shows a comparison between the actual phase functions derived for hexagonal ice crystals and the H-G phase functions derived using the asymmetry factor obtained for each distribution. Compared with the nonspherical ice crystal phase functions, the H-G phase function is smoother and smaller in magnitude in both the forward- and back-scattering directions.
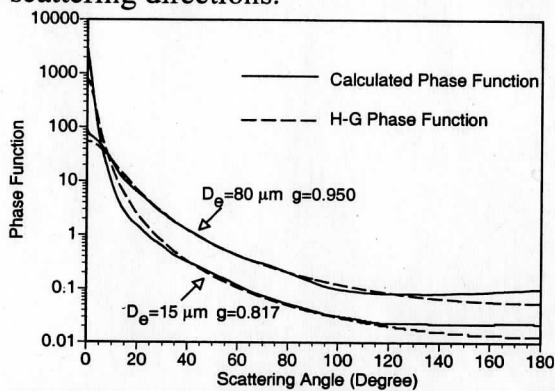

Figure 5. Comparison of the bulk phase function calculated using nonspherical ice habits (droxtals and hexagonal columns) with a Henyey-Greenstein phase function for two effective particle sizes.

Figure 6 shows the differences in the simulated spectral brightness temperatures (converted from the upward spectral flux) at the aircraft level (20 km) between the results derived using the actual phase function derived for nonspherical crystals and the simplified H-G phase function. The brightness temperature using the derived phase function is a little greater than that of the H-G phase function in most cases. This is due to the fact that the forward scattering of derived phase function is usually larger than that of the H-G phase function. The largest differences occur at wavenumbers where strong scattering occurs (1000–1300 cm^{-1}) for large particle effective sizes. For small particles, the difference between the two phase functions is much less, with brightness temperatures generally differing by less than 0.4 K. This may be due to the offset of the difference phase functions within 0-90°. For clouds containing larger ice crystals with a large value of the asymmetry factor, the brightness temperature difference can be more than 1 K. The modified the H-G phase function, such as the double H-G phase function, may offer a better result.
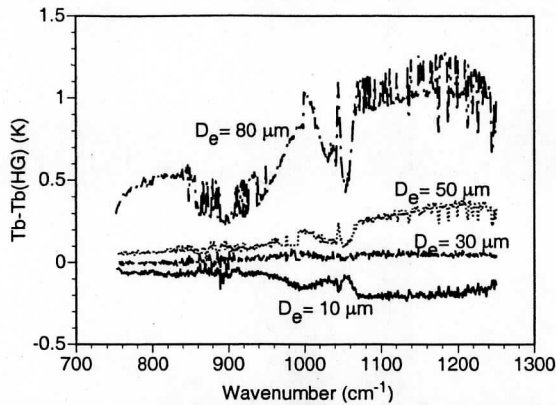
Figure 6. Shown are the differences in the simulated spectral brightness temperatures from use of the actual phase function derived for nonspherical crystals and the simplified H-G phase function in the radiative transfer calculations. Results are shown for simulations of clouds having four effective particle sizes (10, 30, 50, and 80 μm). The calculations are performed at the aircraft altitude (20 km) and assume the US standard atmospheric model; a surface skin temperature of Ts=288.1K; a cloud altitude of 10 km, and an optical thickness τ=1.

Sensitivity study and error analysis

In this section we present the physical basis of the retrieval technique by investigating the sensitivity of high spectral resolution IR brightness temperatures to the effective particle size and optical thickness. As this knowledge will later be used to derive the cloud properties from HIS radiances, we have used an observer altitude of 20 km, the cruising altitude of the ER-2 aircraft, in the upwelling radiance calculations. We also investigate the influence of the atmospheric profiles and the inaccuracies in the cloud temperature and surface skin temperature on the retrieval results.

3.1 Sensitivity of IR Radiance to Effective Particle Size

Figure 7 illustrates the sensitivity of the upwelling brightness temperature spectrum to the ice cloud effective particle size. The spectral brightness temperatures between atmospheric molecular absorption lines (i.e., the atmospheric windows) increase with wavenumber within the 760–1000cm^{-1} region because the absorption of ice crystal particles decreases with wavenumber and the absorption is also size-dependent. The cirrus clouds with smaller effective sizes absorb more radiance underneath in the region of small wavenumbers, leading to a steeper slope for cirrus clouds composed of small particles than for cirrus clouds composed of large particles.
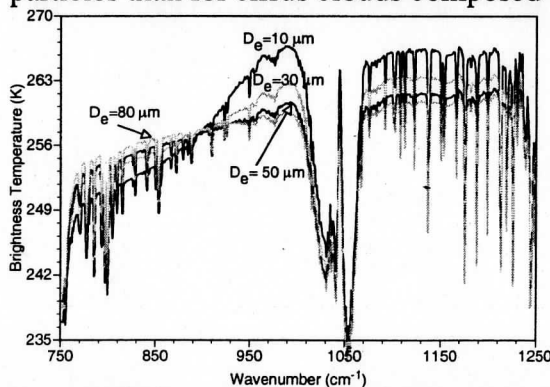

Figure 7. Shown are the spectral brightness temperatures at the aircraft level (20km) as a function of wavenumber for four effective particle sizes (10, 30, 50, and 80 μm). The calculations assume the US standard atmospheric model, a surface skin temperature of 288.1 K, a cloud altitude of 10 km, and an optical thickness τ=1.

From the brightness temperature at atmospheric window wavenumbers, ignoring the strong absorption wavenumbers to remove the absorption lines between 790–960 cm^{-1} and interpolating the brightness temperatures across the gaps, we notice that there is a marked sensitivity in the slope of the observed brightness temperature to the effective particle size (see Fig.8). This sensitivity, in which the slope in brightness temperature increases with decreasing particle size, forms the basis for the inference of effective particle size. We calculate the brightness temperature at the atmospheric windows in the 790–960 cm^{-1} region, and obtain the slope for a range of different effective particle sizes and values of optical thickness.
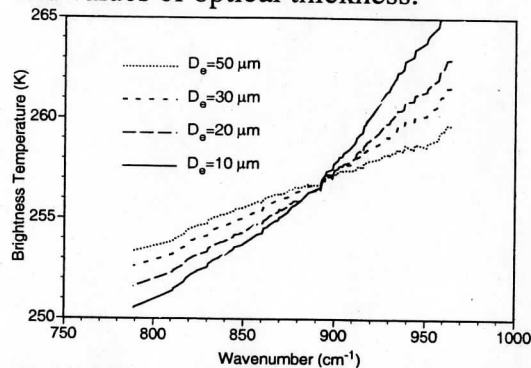
Figure 8. For the spectral region between 790–960 cm^{-1}, the absorption lines between 790–960 cm^{-1} are removed and the resulting window brightness temperatures are interpolated across the gaps. This process more clearly shows how the slope of the observed spectral brightness temperature, with respect to wavenumber, depends upon the effective particle size.

As shown in Fig. 9, the variation of the slope is most sensitive to particle size for small particles and optical thicknesses between 0.4 and 4. For example, for a cloud having an optical thickness of 1, the slope decreases from 9 K/μm to 2 K/μm as the effective particle size increases from 10 μm to 80 μm.
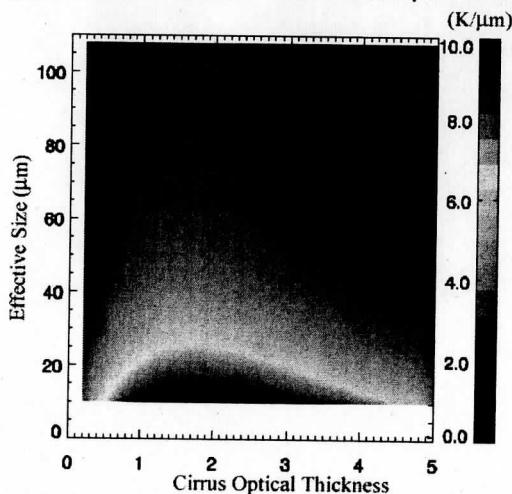

Figure 9. As in Fig. 8, but extended to include both the effect of optical thickness and particle size on the slope of the spectral brightness temperatures and wavenumber between 790–960 cm^{-1}.

3.2 Sensitivity of IR Radiance to Optical Thickness of Clouds

Figure 10 shows simulated upwelling brightness temperature at a 20-km altitude for four values of optical thickness and a fixed effective particle size of 30 μm. The brightness temperature varies with wavenumber between 750–1000 cm^{-1} for small to moderate

optical thicknesses. As shown in Fig. 10, the brightness temperature decreases more than 40 K as the optical thickness increases from 0.5 to 5. For optically thick ice clouds (optical thickness larger than 5), the brightness temperature has less dependence on wavenumber.
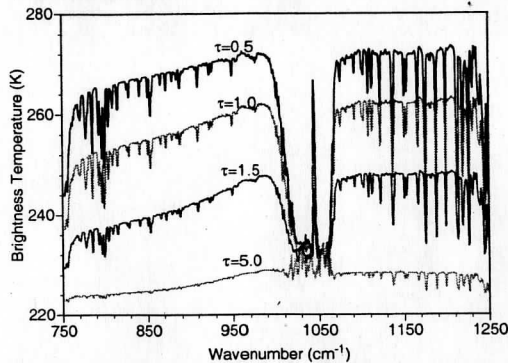

Figure 10. Same as Fig. 7, but for the sensitivity of spectral brightness temperature to the cloud optical thickness. The assumed effective particle size is fixed at 30 μm.

3.3. Error Analysis

The brightness temperature discretization in Fig. 9 is 0.5 K/μm. If we assume the minimum measurable temperature difference is 1 K then the effective particle size cannot be accurately retrieved if the variation of brightness temperature difference between 950 and 790 cm^{-1} is less than 1 K due to the variation of the effective particle size. Further theoretical error analysis suggested that, for a threshold of 0.5 K/μm, the maximum retrievable effective size is no larger than 80 μm with an uncertainty of 10 μm. The uncertainty decreases to about 2 μm when the effective size is 10 μm. Similarly, the maximum retrievable optical thickness is approximately 8 with an uncertainty of 1. For the case of a visible optical thickness of 1, the uncertainty decreases to less than 0.1.

In the IR spectrum, the surface skin temperature, cloud temperature and atmospheric profile contributed significantly to the top of atmosphere radiance. Hence, in the remains of the section, we study the effects of uncertainties in surface and cloud temperature to retrieval results. We also investigate the variation of the sensitivity for different atmospheric profiles.

3.4 Effects of Surface and Cloud Temperature on Retrieval Accuracy

In this section we analyze the effects of inaccurate surface and cloud temperature that are provided as inputs to the algorithm, on the accuracy of the inferred microphysical and optical properties. Cloud-top pressure or temperature may be inferred by methods such as the CO_2 slicing method [48] or by the minimum local emissivity variance (MLEV) method [49]. The MLEV algorithm uses a physical approach in which the local spectral variances of cloud emissivity are calculated for a number of assumed cloud pressures. The optimal cloud emissivity spectrum is that which has the minimum local emissivity variance among the retrieved emissivity spectra associated with different assumed cloud pressures. This technique is based on the observation that the absorption, reflection, and scattering processes of clouds exhibit relatively limited localized spectral emissivity structure in the 750–1250 cm^{-1} spectral region. Any retrieved cloud emissivity that exhibits spectral variation similar to that of carbon dioxide and water vapor absorption is indicative of an incorrect specification of cloud pressure level and its associated spectral emissivity. MLEV analysis shows that cloud pressure root mean square errors for a single

layer cloud with effective cloud emissivity greater than 0.1 are ~30 hPa, ~10 hPa, and ~50 hPa, for high, middle, and low clouds, respectively.

Errors in the assigned cloud pressure and its corresponding temperature will affect the retrieval of optical thickness. Figure 11 shows the predicted error in the retrieved optical thickness as a function of cloud temperature error. The error of cloud temperature is assumed to be within ±7 K, corresponding to the variation of temperature at a cloud altitude of 10±1 km. A lower-than-actual cloud temperature will result in an overestimate of the optical thickness, while a higher-than-actual cloud temperature will lead to an underestimate of optical thickness. The impact of the cloud temperature error is more pronounced for optically thick ice clouds than for optically thin ice clouds. Generally, the error in the retrieved optical thickness is less than 10% if the cloud temperature is within ±5 K of the true temperature and the cloud optical thickness is less than 2.
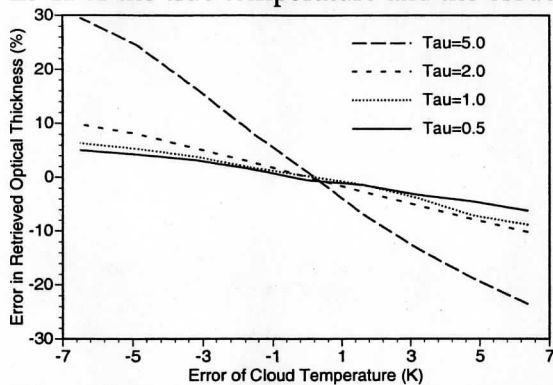

Figure 11. Errors in retrieved optical thickness resulting from an error in cloud temperature for four optical thicknesses. The ice cloud has an effective particle size of 25 μm. The actual cloud temperature is assumed to be 223.3 K, but varies from 229.7 to 216.8 K.

Figure 12 shows the relationship between the retrieved effective particle size and the cloud temperature error. Different cloud temperatures result in different brightness temperature slopes, and thus lead to effective particle size retrieval errors. The error is within ±15% if the cloud temperature error is within ±5 K.
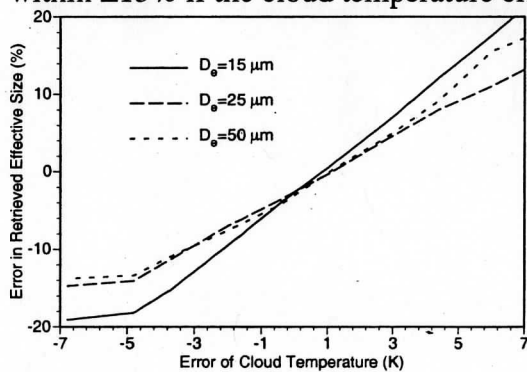

Figure 12. Errors in retrieved effective size to the error of cloud temperature for 3 effective particle sizes. The ice cloud has an optical thickness of 1.

Figure 13 shows the error in retrieved optical thickness as a function of surface skin temperature error. An error in the surface skin temperature has a pronounced influence on the retrieval of optical thickness if the cloud is optically thin, because the upwelling radiation is primarily from the surface, with some modest attenuation by the atmosphere and cloud. For very thick clouds, an error in the surface skin temperature has little influence on the retrieved optical thickness. For the retrieval accuracy of optical

thickness (Fig. 13) to be better than 10%, the surface skin temperature error should be less than ±2.5 K.
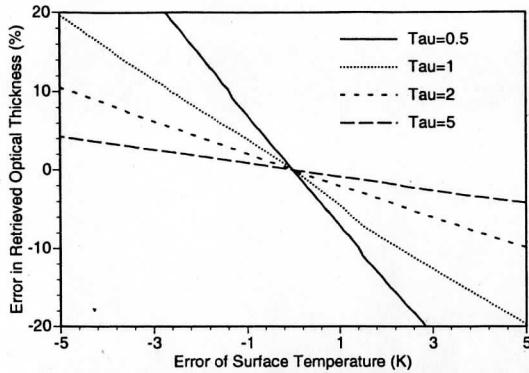

Figure 13. Errors in retrieved optical thickness resulting from an error in surface skin temperature for four cloud optical thicknesses. The ice cloud has an effective particle size of 25 μm and is located at an altitude of 10 km.

Figure 14 shows the dependence of the retrieved error in effective particle size on the error in surface skin temperature. Compared to the results in Fig. 13, an error in surface skin temperature (Fig. 14) has less influence on the effective particle size than on the optical thickness, because the variation of the surface skin temperature does not change as much with the slope of brightness temperature between 790–960cm^{-1}. If the error of surface skin temperature is within ±2.5 K, the error of retrieved effective particle size will be within ±5%.
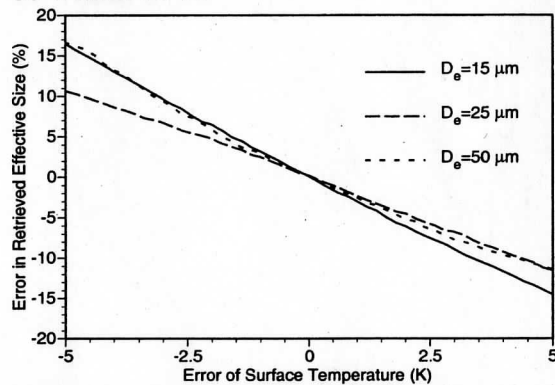

Figure 14. Errors in retrieved effective size caused by an error in surface skin temperature for three effective particle sizes. The cloud optical thickness is constant at 1, and the cloud altitude is 10 km.

3.5 Effect of the Atmospheric Profiles

We now investigate the sensitivity of the brightness temperature to different regional average atmospheric profiles by calculating the brightness temperature difference between clear-sky and cloudy radiance, defined as the cloud forcing. Figure 15 shows the cloud forcing for both a climatological tropical (TRO) and subarctic winter (AW) atmosphere for two assumed values of cloud optical thickness. We assume the surface skin temperature is the same as the atmospheric temperature of the lowest layer, that is, 300 K (tropical) and 257.1 K (subartic winter). Because the upwelling brightness temperature for the subarctic winter atmosphere is much lower than that of the tropical atmosphere, the sensitivity decreases for the subarctic winter atmosphere relative to a warmer tropical atmosphere (I'm not sure I agree with this – is not just a result of the

temperature of the cloud and the temperature of the surface/atmosphere are more similar in the artic case?). Even for the subartic winter atmopsheric model, however, the variation of cloud forcing can still be more than 20 K when the optical thickness increases from 0.5 to 2. Thus, the IR spectra still contains sufficient information in these conditions from which the properties of ice clouds can be inferred using the simultaneous retrieval technique.
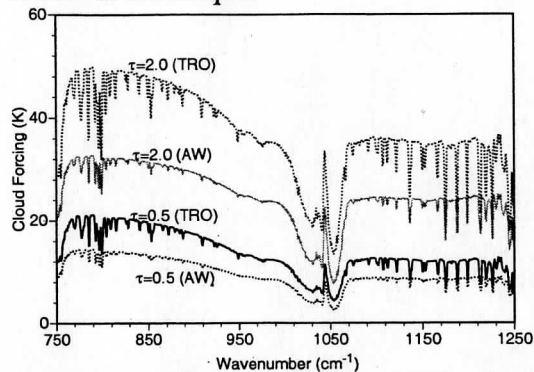

Figure 15. Sensitivity of cloud forcing (brightness temperature difference between clear and cloudy sky) to the atmospheric model for two cloud optical thicknesses.

4. Inference of Ice Cloud Microphysical and Optical Properties

4.1 Simultaneous Retrieval Algorithm

An understanding of the above dependence of the upwelling radiance to cloud properties leads us to the following methodology for simultaneous retrieval of effective particle size and optical thickness. First, the clear-sky atmospheric optical thickness profile is calculated with the LBL radiative transfer code. Given an ice cloud height and temperature, a series of spectral radiances are simulated using DISORT for a range of cloud effective particle sizes and optical thicknesses, and additional pre-calculated cloud optical properties discussed in Section 2.1. By matching the slope of brightness temperature in the 790–960 cm^{-1} band to the observed spectrum, the effective particle size of the ice cloud D_e can be estimated (note that, at this initial stage, a first-guess optical thickness τ is used). Then the optical thickness is derived by comparing the observed spectrum to the simulations in 1100–1250 cm^{-1} band with the values of D_e determined in the previous step. The final particle size and optical thickness are obtained by iteration until the differences are minimized between the observed and simulated IR spectrum. A best-fit value is reached when the difference (variance) between the observed and simulated IR spectrum within the two bands is minimal.

In the following section, we apply the simultaneous retrieval algorithm outlined above to HIS data collected from two field experiments.

4.2 Case study 1: FIRE-ACE Experiment

During FIRE-ACE [50], upwelling spectral radiance was observed by the HIS instrument onboard the ER-2 aircraft from an altitude of 20 km. HIS data from Band 1 (750–1080 cm^{-1}) and Band 2 (1100–1250 cm^{-1}) were selected for analysis between 2345 UT and 0020 UT on 22–23 May 1998. This period provides example observations for water clouds (before 0007 UT), clear sky (0007 to 0010 UT), and high ice clouds (after 0010 UT). The data were recorded in Alaska near 67.52°N, 150.60°W. Figure 16 shows the Cloud Lidar System (CLS) imagery for this period which provides information on the cloud-top altitude [51] and was used together with a MODIS Airborne Simulator (MAS)

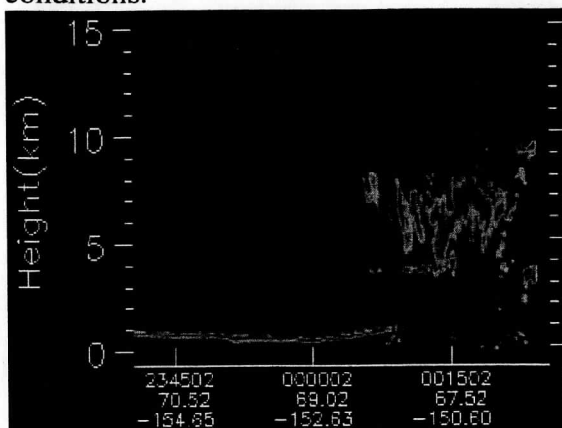image (not shown here) to discriminate between clear sky, water cloud and ice cloud conditions.

Figure 16. Cloud Lidar System (CLS) imagery providing information on cloud heights and boundaries. The scanning times, given in the format HH:MM:SS, used in this paper are 00:05:23 for the water cloud data, and 00:17:01 for ice cloud data. Scanning locations in degrees latitude and longitude are given below the time values.

The HIS brightness temperature spectrum for clear sky (0009 UT) is shown in Fig. 17, while those for water clouds (0005 UT) and high ice clouds (0017 UT) are shown in Fig. 18. Also plotted on these two figures are the best-fit simulated radiances that were generated from temperature, pressure and relative humidity data from a nearby rawinsonde at 2324 UT on May 22 1998, together with cloud properties determined using our retrieval technique. It should be pointed that the atmospheric parameters, particular the surface skin temperature and cloud temperature, are important to the retrieval as studied in previous section. The *in-situ* real time temperature profile should be used for the retrieval if possible.
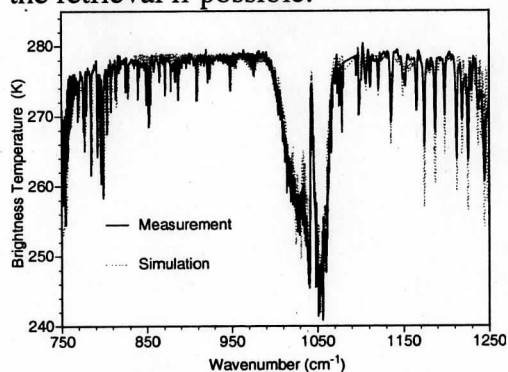

Figure 17. Observed and simulated IR upwelling spectra under clear-sky conditions for 23 May 1998, 00:09:04 UT; surface skin temperature is 279 K.

Fig. 18 demonstrates that the observed spectral signature of the ice cloud is quite different from that of the water cloud. The brightness temperature of the ice cloud increases with wavenumber over the $750-1000 cm^{-1}$ region. This expected result, as previously mentioned, is due to the spectral variation of the absorption of ice crystals.
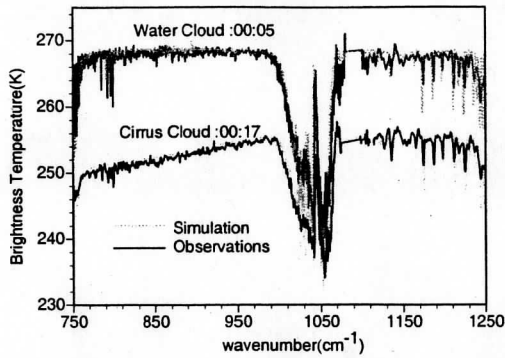
Figure 18. The observed and simulated upwelling IR spectra for ice and water cloud conditions (the number in the figure is given in the format HH:MM UT on May 23 1998).

Fig. 19 illustrates the process of matching the simulated and observed brightness temperatures by varying (and thus, when the brightness temperatures match, retrieving) the cloud properties in the simulations. The left panel of Fig.19 shows comparisons of the observed HIS spectrum (solid black curve) with simulated brightness temperatures for a number of trial effective particle sizes D_e=35, 45, and 60 μm and a first-guess optical thickness τ =1.43, within the 760–1000 cm^{-1} band. The right panel of Fig.19 shows brightness temperatures for the best-matched effective particle size D_e=45.0 μm (as determined from the previous step as illustrated in left panel of Fig.19) with trial optical thickness values τ =1.2, 1.43, and 1.6 within the 1100–1250 cm^{-1} band). The effective cloud particle size is retrieved by fitting a line between 790–960 cm^{-1}. The resultant values of the effective particle size and optical thickness in this case are therefore 45 μm and 1.43 respectively.
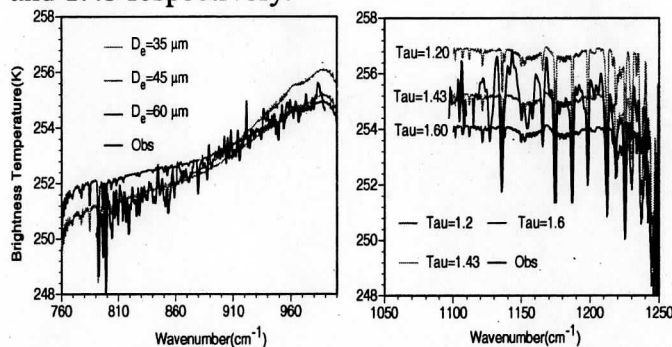

Figure 19. The simultaneous retrieval of the effective size and optical thickness of ice clouds from HIS spectra. (a) Brightness temperature versus particle size assuming τ=1.43. (b) Brightness temperature versus optical thickness assuming D_e=45 μm. Date: 23 May 1998, 00:17:01 UT. The surface skin temperature is 267.6 K, and the cloud altitude is 7.0 km.

4.3 Case Study 2: SUCCESS Experiment (small particle case)

Smith et al. [2] reported a strong absorption signature of very small cirrus cloud particles during SUCCESS in 1996. Figure 20 shows the HIS spectrum collected from the ER-2 during an overflight of a jet aircraft contrail, which generally consists of very small particles. The best-fit simulated spectral brightness temperatures, also plotted, are simulations for an ice cloud model based solely on droxtals with an effective particle size of 12.5 μm, and an optical thickness of 1.60. The simulation generally agrees well with the observed spectrum (except at 990 cm^{-1}, probably due to the residual effect of an imperfect ozone concentration profile) and indicates that the droxtal crystal habit seems to be a realistic approximation for small ice particles. *Chung et al.* [14] calculated the

spectrum for this case by assuming that ice clouds are composed of spherical ice particles with an assumed Gamma size distribution. The retrieved effective radius (7.35 μm) and IWP (6.85 g/m^2) is equivalent to an optical thickness of 1.5. Our retrieved optical thickness is close to Chung's result, but the effective particle size is a little smaller. The differences are due to the more complex ice habit (droxtal) used in our study. A droxtal with the same maximum dimension will have smaller effective size than the ice sphere. Thus, the retrieved effective size is a little small by assuming the droxtal instead of sphere. The effect of ice crystal nonsphericity deserves a further study.
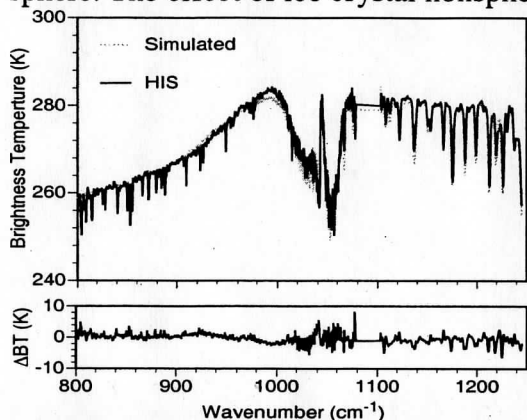

Figure 20. The comparison of observed and simulated upwelling IR spectra at 20 km altitude for a jet contrail composed of primarily small ice particles (D_e=12.5 μm, τ =1.6).

5. Summary

Within the 750–1000 cm^{-1} spectral region, the slope of brightness temperature is sensitive to ice crystal effective particle size, particularly for small particles. At wavenumbers between 1100 and 1250 cm^{-1}, the spectrum is more sensitive to the optical thickness than to particle size. Thus, using the terrestrial window information within the 750–1250 cm^{-1} spectral band, we can infer the optical thickness and effective particle size for ice clouds simultaneously.

While the error analysis shows that the uncertainty of the retrieved optical thickness and effective particle size exhibits a small variation. The error for retrieving particle size in conjunction with an uncertainty of 5 K in cloud temperature, or a surface temperature uncertainty of 2.5 K, is less than 15%. The corresponding error in the uncertainty of optical thickness is within 5-20%, depending on the value of cloud optical thickness. The maximum effective particle size that may be retrieved with the present approach (i.e., an upper limit) is 80 μm with an uncertainty of approximately 10 μm at D_e=80 μm, and about 2 μm uncertainty at D_e=10 μm. The maximum retrievable optical thickness is approximately 8 with an uncertainty of 1. For the case of optical thickness 1, the uncertainty decreases to less than 0.1.

The applicability of the technique is demonstrated using the aircraft–based HIS data from the SUCCESS in 1996 and FIRE-ACE in 1998. Both larger (45 μm) and smaller (12.5 μm) effective particle sizes simultaneous retrievals yield reasonable fit to the observed spectra. Spectral temperature differences of ~4 degree and >20 degree Kevin (the slope of the spectral brightness temperatures and wavenumber between 790–960 cm^{-1}) further demonstrate the forward modeling of cloudy measurements and retrieval algorithm is capability of obtaining reliable cloud property. Subsequent cloud modeling study and retrieval analysis verification using space-borne and active cloud measurements, and *in-situ* measurements will be conducted to advance our ability to refine this technique.

References

[1] D. K. Lynch, K. Sassen, D. O. Starr and G. Stephens (Eds.), Cirrus, (Oxford Univ. Press, New York, 2002)

[2] W. L. Smith, S. Ackerman, H. Revercomb, H. Huang, D. H. DeSlover, W. Feltz, L. Gumley and A. Collard, "Infrared spectral absorption of nearly invisible cirrus clouds," *Geophys. Res. Lett.*, VOL. *25*, pp.1137–1140, 1998.

[3] G. L. Stephens, S.C. Tsay, P.W. Flatau, "The relevance of microphysical and radiative properties of cirrus clouds to climate and clime feedback," *J. Atmos. Sci.*, vol. 47, pp.1742-1753, 1990.

[4] K. N. Liou, "Influence of cirrus clouds on weather and climate processes: A global perspective," *Mon. Wea. Rev.*, vol. 114, pp.1167-1199, 1986.

[5] T. Nakajima and M. D. King, "Determination of the Optical Thickness and Effective Particle Radius of Clouds from Reflected Solar Radiation Measurements. Part I: Theory," *J. Atmos. Sci*, vol.47, pp. *1878-1893*, 1990.

[6] M. D. King, W. P. Menzel, Y. J. Kaufman, D. Tanré, B. C. Gao, S. Platnick, S. A. Ackerman, L. A. Remer, R. Pincus, and P. A. Hubanks, "Cloud and Aerosol Properties, Precipitable Water, and Profiles of Temperature and Humidity from MODIS," *IEEE Trans. Geosci. Remote Sens.*, vol.41, pp.442-458, 2003.

[7] S. Platnick, M.D. King, S. A. Ackerman, W. P. Menzel, B.A. Baum, J. C. Riédi, and R. A. Frey, "The MODIS Cloud Products: Algorithms and Examples from Terra. IEEE Transactions on Geoscience and Remote Sensing," *IEEE Trans. Geosci. Remote Sens.*, vol.41, pp.459-473, 2003.

[8] C.J. Stubenrauch, R. Holz, A. Chedin, D.L. Mitchell, A.J. Baran, "Retrieval of cirrus ice crystal sizes from 8.3 and $11.1\mu m$ emissivities determined by the improved initialization inversion of TIROS-N operational vertical sounder observations," *J Geophys Res*, vol.104, pp.793–808, 1999.

[9] P. Zuidema, "Convective Clouds over the Bay of Bengal," *Mon. Wea. Rev.*, vol.131, pp. 780-798, 2003.

[10] Smith, W. L., D. K. Zhou, F. W. Harrison, H. E. Revercomb, A. M. Larar, H.-L. Huang, and B. Huang, 2000: Hyperspectral remote sensing of atmospheric profiles from satellites and aircraft, Proceedings of SPIE, William L. Smith and Yoshifumi Yasuoka, editors. *Hyperspectral Remote Sensing of the Land and Atmosphere.* 9-12 Oct. 2000, 94-102.

[11] Huang, H.-L., H. E. Revercomb, J. Thom, P. B. Antonelli, B. Osborne, D. Tobin, R. Knuteson, R. Garcia, S. Dutcher, J. Li, and W. L. Smith, 2000: Geostationary Imaging FTS (GIFTS) Data Processing: Measurement Simulation and Compression. Proceedings of SPIE, William L. Smith and Yoshifumi Yasuoka, editors. *Hyperspectral Remote Sensing of the Land and Atmosphere.* 9-12 Oct. 2000, 103-114.[12] Glumb R. J., D. C. Jordan, P. Mantica, 2002: Development of the Crosstrack Infrared Sounder (CrIS) sensor design. Proceedings of SPIE, Infrared Spaceborne Remote Sensing IX; Marija Strojnik, Bjorn F. Andresen; Editors. Proc. SPIE Vol. 4486, p. 411-424.

[13] S. Ou, K. N. Liou, P. Yang, P. Rolland, T. R. Caudill, J. Lisowski, and B. Morrison, "Airborne retrieval of cirrus cloud optical and microphysical properties using ARES $5.1-5.3\mu m$ channel data," *J. Geophys. Res.*, vol.103, pp.23231-23242, 1998

[14] S. Chung, S. Ackerman, P. F. Van Delst, and W. P. Menzel, "Model calculations and interferometer measurements of ice-clouds characteristics," *J. Appl. Meteor.*, vol. *39*, pp.634–644, 2000.

[15] S. A. Ackerman, W. L. Smith, J. D. Spinhirne, and H. E. Revercomb, "The 27-28 October 1986 FIRE IFO cirrus case study: Spectral properties of cirrus clouds in the 8-12 µm window," *Mon. Wea. Rev.*, vol.118, pp.2377-2388, 1990.

[16] R.J. Bantges, J. E. Russell, and J. D. Haigh, "Cirrus cloud top-of-atmosphere radiance spectra in the thermal infrared," *J. Quant. Spectrosc. Radiat. Transfer*, vol.63, pp. 487–498, 1999.

[17] D. H. DeSlover, W. L. Smith, P. K. Piironen, and E. W. Eloranta, "A methodology for measuring cirrus cloud visible-to-infrared spectral optical thickness ratios," *J. Atmos. Oceanic Technol.*, vol.16, pp.251–262, 1999.

[18] B.H.K. Kahn, A. Eldering, F. W. Irion, F. P. Mills, B. Sen, and M. R. Gunson, "Cloud identification in Atmospheric Trace Molecule Spectroscopy infrared occultation measurements," *Appl. Opt.*, vol. 41, pp.2768–2780, 2002.

[19] A. Eldering, F. W. Irion, A. Y. Chang, M. R. Gunson, F. P. Mills, and H. M. Steele, "Vertical profiles of aerosol volume from high-spectral-resolution infrared transmission measurements," I. Methodology, *Appl. Opt.*, vol. 40, pp.3082–3090, 2001.

[20] C. Rathke and J. Fischer, "Retrieval of cloud microphysical properties from thermal infrared observations by a fast iterative radiance fitting method," *J. Atmos. Oceanic Technol.*, vol. 17, pp.1509–1524, 2000.

[21] M.D. Chou, K.T. Lee, S. C. Tsay, and Q. Fu, "Parameterization for cloud longwave scattering for use in atmospheric models," *J. Climate*, vol.12, pp.159-169,1999.

[22] A. J. Heymsfield and C. M. R. Platt, "A parameterization of the particle size spectrum of ice clouds in terms of the ambient temperature and the ice water content," *J. Atmos. Sci.*, vol.41, pp.846–855, 1984.

[23] A. J. Heymsfield and J. Iaquinta, "Cirrus crystal terminal velocities," *J. Atmos. Sci.*, vol.5, pp.916–938, 2000.

[24] P. Yang, B. A. Baum, A. J. Heymsfield, Y. X. Hu, H.-L. Huang, S.-Chee Tsay, and S. Ackerman, "Single-scattering properties of droxtals," *J. Quant. Spectrosc. Radiat. Transfer.* vol. 79–80, pp.1159–1169, 2003.

[25] P. Yang, B. C. Gao, B. A. Baum, Y. X. Hu, W. J. Wiscombe, S. C. Tsay, D. M. Winker, and S. L. Nasiri, "Radiative properties of cirrus clouds in the infrared (8–13 μm) spectral region," *J. Quant. Spectrosc. Radiat. Transfer*, vol.70, pp.473–504, 2001.

[26] .P. Yang, and K. N. Liou, "Finite-difference time domain method for light scattering by small ice crystals in three-dimensional space," *J. Opt. Soc. Amer.*, vol. A13, pp. 2072-2085, 1996.

[27] W. J. Wiscombe, "Improved Mie scattering algorithms," *Appl. Opt.*, vol.19, pp.1505–1509, 1980.

[28] Q. Fu, W.B. Sun, P.Yang, "On modeling of scattering and absorption by cirrus nonspherical ice particles at thermal infrared wavelengths," *J. Atmos Sci*, vol.56, pp.2937–2947,1999.

[29] P. Yang and K. N. Liou, "Geometric-Optics-integral-equation method for light scattering by nonspherical ice crystals," *Appl. Opt.*, vol.35, pp.6568-6584,1996

[30] P. Yang, B.-C. Gao, B. A. Baum, W. Wiscombe, M. I. Mischenko, D. M. Winker, and S. L. Nasiri, Asymptotic solutions of optical properties of large particles with strong absorption. *Appl. Opt.*, vol.40, pp.1532-1547, 2001

[31] Y.K. Lee, P. Yang, M.I. Mishchenko, B. A. Baum, Y. Hu, H.-L. Huang, W.J. Wiscombe, and A. J. Baran, "On the use of circular cylinders as surrogates for hexagonal pristine ice crystals in scattering calculations at infrared wavelengths," *Appl. Opt.* vol.42, pp. 2653-266,2003

[32] M. I. Mishchenko and L. D. Travis, Capabilities and limitations of a current FORTRAN implementation of the T-matrix method for randomly oriented rotationally symmetric scatters, *J. Quant. Spectrosc. Radiat. Transfer*, 60, 309-324, 1998.

[33] Q. Fu, P. Yang and W. B. Sun, "An accurate parameterization of the infrared radiative properties of cirrus clouds for climate models," *J. Climate*, vol.25, pp.2223–2237, 1998.

[34] D.L.Mitchell, S.K.Chai, Y.Liu, A.J.Heymsfield, Y.Dong, "Modeling cirrus clouds. PartI: treatment of bimodal size spectra and case study analysis," *J. Atmos. Sci.* vol.53, pp.2952 –2966,1996.

[35] . Q. Fu and W. B. Sun, "Retrieval of cirrus particle sizes using a split-window technique: a sensitivity study, " *J. Quant. Spectrosc. Radiat. Transfer*, vol. 70, pp.725–736, 2001.

[36] W. P. Arnott, Y. Y. Dong , and J. Hallett, "Extinction efficiency in the infrared (2-18 μm) of laboratory ice clouds: observations of scattering minimum in the Christiansen bands of ice," *Appl. Opt.* , vol.34, pp.541–551, 1995.

[37] P. Yang, K. N. Liou and W. P. Arnott, "Extinction efficiency and single-scatttering albedo for laboratory and natural cirrus clouds," *J. Geophys. Res.*, vol. 103, pp.825–835, 1997.

[38] J.E. Hansen and L.D. Travis, "Light scattering in planetary atmospheres," Space Sci. Rev., vol.16,pp527-610,1974.

[39] M.D. Chou, and L. Kouvaris, "Monochromatic calculations of atmospheric radiative transfer due to molecular line absorption," *J. Geophys. Res.*,vol. 91, pp.4047-4055, 1986.

[40] L. S. Rothman, C. P. Rinsland, A. Goldman et al., "The HITRAN Molecular Spectroscopic Database and HAWKS (HITRAN Atmospheric Workstation): 1996 Edition," *J. Quant. Spectrosc. Radiat. Transfer*, vol. 60, pp. 665–710, 1998.

[41] J. F. Kielkopf, "New Approximation to the Voigt Function with application to spectral line profiles," *J. Opt. Sci. Am.*, vol. 63, pp.987–995, 1973.

[42] D. C. Tobin, F. A. Best, S. A. Clough, R. G. Dedecker, R. G. Ellingson, R. K. Garcia, H. B. Howell, R. O. Knuteson, E. J. Mlawer, H. E. Revercomb, J. J. Short, P. F. W. van Delst, and V. P. Walden, "Downwelling spectral radiance observations at the SHEBA ice station: Water vapor continuum measurements from 17–26 μm, " *J. Geophys. Res.*, vol. 104, pp.2081–2092, 1999.

[43] K. Stamnes, S. C. Tsay, W. Wiscombe and K. Jayaweera, "A numerically stable algorithm for discrete-ordinate-method radiative transfer in multiple scattering and emitting layered media," *Appl. Opt.*, vol. 27, pp.2502–2509, 1988.

[44].Y. X. Hu, B Wielicki, B. Lin, G. Gibson, S. C. Tsay, K. Stamnes, and T. Wong, "Delta-fit: A fast and accurate treatment of particle scattering phase functions with weighted singular-value decomposition least-square fitting," J. Quant. Spectrosc. Radiat. Transfer, vol. 65, pp.681-690, 2000.

[45] M.I. Mishchenko, J. W. Hovenier, and L. D. Travis (Eds.), *Light Scattering by Nonspherical Particles: Theory, Measurements, and Applications*, San Diego, Academic Press, 2000.

[46] M. I. Mishchenko, W. B. Rossow, A. Macke, and A. A. Lacis, "Sensitivity of cirrus cloud albedo, bidirectional reflectance, and optical thickness retrieval to ice-particle shape," *J. Geophys. Res.*, vol.101, pp.16973-16985,1996.

[47] Y. Takano, K. N. Liou, and P. Minnis, "The effects of small ice crystals on cirrus infrared radiative properties," *J. Atmos. Sci.*, vol.49, pp.1487-1493,1992

[48] D. P. Wylie and W. P. Menzel, "Eight years of global high cloud statistics using HIRS," *J. Climate,* vol. 12, pp.170–184,1999.

[49] H. L. Huang, W. L. Smith, J. Li, P. Antonelli, X. Wu, R. O. Knuteson, B. Huang, and B. J. Osborne, "Minimum local emissivity variance retrieval of cloud altitude and effective spectral emissivity simulation and initial verification," accepted by *J. Appl. Meteo.*, 2003.

[50] J. A. Curry, P. V. Hobbs, M. D. King, D. A. Randall, P. Minnis, G. A. Isaac, J. O. Pinto, T. Uttal, A. Bucholtz, D. G. Cripe, H. Gerber, C. W. Fairall, T. J. Garrett, J. Hudson, J. M. Intrieri, C. Jakob, T. Jensen, P. Lawson, D. Marcotte, L. Nguyen, P. Pilewskie, A. Rangno, D. C. Rogers, K. B. Strawbridge, F. P. J. Valero, A. G. Williams, and D. Wylie, "FIRE Arctic Clouds Experiment," *Bull. Amer. Meteor. Soc.*,vol.81, pp.5–29, 2000.

[51] J. D. Spinhirne and W. D. Hart, "Cirrus structure and radiative parameters from airborne lidar and spectral radiometer observations," *Mon. Wea. Rev.*, vol.118, pp.2329–2343, 1990.